9-2-2017

INTERACTION BETWEEN WATER AND PLANTS: RICH DYNAMICS IN A SIMPLE MODEL

Xiaoli Wang
wxl711@swu.edu.cn

Junping Shi
College of William and Mary, shij@math.wm.edu

Guohong Zhang
College of William and Mary, zgh711@swu.edu.cn

Recommended Citation

Wang, Xiaoli; Shi, Junping; and Zhang, Guohong, INTERACTION BETWEEN WATER AND PLANTS: RICH DYNAMICS IN A SIMPLE MODEL (2017). *DISCRETE AND CONTINUOUS DYNAMICAL SYSTEMS-SERIES B*, 22(7).
10.3934/dcdsb.2017159

DISCRETE AND CONTINUOUS
DYNAMICAL SYSTEMS SERIES B
Volume **22**, Number **7**, September **2017**

doi:10.3934/dcdsb.2017159

pp. **2971–3006**

INTERACTION BETWEEN WATER AND PLANTS: RICH DYNAMICS IN A SIMPLE MODEL

Xiaoli Wang

School of Mathematics and Statistics, Southwest University
Chongqing, 400715, China

Junping Shi*

Department of Mathematics, College of William and Mary
Williamsburg, VA 23187-8795, USA

Guohong Zhang

School of Mathematics and Statistics, Southwest University
Chongqing, 400715, China

(Communicated by Sze-Bi Hsu)

Abstract. An ordinary differential equation model describing interaction of water and plants in ecosystem is proposed. Despite its simple looking, it is shown that the model possesses surprisingly rich dynamics including multiple stable equilibria, backward bifurcation of positive equilibria, supercritical or subcritical Hopf bifurcations, bubble loop of limit cycles, homoclinic bifurcation and Bogdanov-Takens bifurcation. We classify bifurcation diagrams of the system using the rain-fall rate as bifurcation parameter. In the transition from global stability of bare-soil state for low rain-fall to the global stability of high vegetation state for high rain-fall rate, oscillatory states or multiple equilibrium states can occur, which can be viewed as a new indicator of catastrophic environmental shift.

1. **Introduction.** In the past four decades, the disappearance of vegetation which is referred as desertification has become a serious environmental problem, and the global ecosystems are threatened today more than ever before [7]. Biologically it indicates the ecological unbalance between the limited water resource and ecosystem engineers such as animals, plants or microorganisms [12, 13]. How ecosystem engineers affect ecosystems is one of the main frontiers in ecology [25] and it has fascinated many ecologists [7, 12, 13]. The disappearance of vegetation may be a slow and gradual process in many forms, such as spotted vegetation patches, fairy rings, tiger bush bands, and bands, which have been reported and studied in different environment [15, 14, 22, 23, 25, 28]. Mathematically it means formation

2010 *Mathematics Subject Classification.* Primary: 34C23, 34C60, 37G15, 92D40.

Key words and phrases. Water-plant model, bistability, Hopf bifurcations, Bogdanov-Takens bifurcations, homoclinic bifurcations, closed loop of cycles.

X.-L. Wang is partially supported by grants from National Science Foundation of China (11671327), the Ph.D. Foundation of Southwest University (SWU116069); J.-P. Shi is partially supported by US-NSF grants DMS-1313243; G.-H. Zhang is partially supported by grants from National Science Foundation of China (11461023), Fundamental Research Funds for the Central Universities(XDJK2016C121).

* Corresponding author: Junping Shi.

of non-uniform spatiotemporal patterns, such as symmetry breaking, instabilities, and coexistence of stable states [7]. Pattern formation in water-plant systems in the semi-arid climatic zone has been investigated by many authors [17, 31] with the applicability of Turing's idea [30]. The dynamic of this class of water-plant systems is governed by the competition of plants (shrubs, trees) for common resource (water, light) which admits spatial dynamics. The corresponding reaction-diffusion systems undergo a Turing-like stability change, which means a uniform steady state is stable with respect to the ordinary differential equation system but unstable with respect to the corresponding reaction-diffusion system, that may generate spotted vegetation patches, fairy rings, tiger bush bands, and bands in some parameter range.

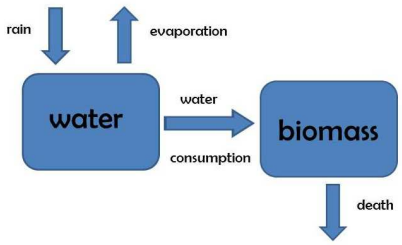

FIGURE 1. A water-plant interaction system with the infiltration feedback.

Understanding the underlying mechanism for generation of vegetation patterns and their observed resilience is considered as an important step toward a comprehension of the desertification process, where environmental effects such as climate changing and grazing destroy the natural balance toward stable aridity [28]. Vegetation pattern formation is a complex process involving not only the spatial physical movement of substance described by diffusion, advection and chemotaxis, but also the chemical interactions between resource and biomass. In this article, we propose a model of ordinary differential equations of water and biomass, based on a previous model proposed in Shnerb et al. [28] describing interaction of one plant species (shrubs or trees) and one resource. We show that the proposed two-dimensional simple ODE model possesses surprisingly rich dynamics including multiple stable equilibria, backward bifurcation of positive equilibria, supercritical or subcritical Hopf bifurcations, bubble loop of limit cycles, homoclinic bifurcations and saddle-node bifurcation. This model will serve as the kinetic model for our subsequent studies of spatiotemporal pattern formation for the corresponding partial differential equation model with effect of diffusion, advection and cross-diffusion.

Based on the model in [28], we propose a nondimensionalized water-biomass model in the following form

$$\begin{cases} \dfrac{dw}{dt} = R - \lambda wb - w, \\ \dfrac{db}{dt} = wb - \mu(b)b. \end{cases} \tag{1}$$

Here $w(t)$ is the amount of available water and $b(t)$ is the amount of shrubs biomass; R is the rain-fall rate; the term $-w$ represents water losses by percolation and evaporation; the term wb represents growth of shrubs as they consume water, while $-\lambda wb$ is the corresponding consumption of water by shrubs and λ is the water

consumption rate in the presence of biomass; $\mu(b)b$ is the biomass death rate. A flow diagram for (1) is shown in Figure 1. In [28], a reaction-diffusion type system was proposed with the kinetic system (1) with $\mu(b) \equiv \mu$ (a constant), and they showed that no Turing-like instability can occur for that system. In this study, we consider a biomass per capita death rate in the following form [20] (see Figure 2)

$$\mu(b) = \mu_0 + \frac{\mu_1}{b+1}, \tag{2}$$

where μ_0 and μ_1 are positive constants. Here $\mu(b)$ is assumed to be a decreasing function of biomass b in order to capture the infiltration feedback [6, 7]. Biologically it can be explained as follows. The biomass can improve the soil environment locally which in turn increases infiltration at vegetation patch. Thus the larger biomass density results in the higher infiltration and the more soil water available and the smaller death rate of the biomass, whereas upon a constant death rate μ_0.

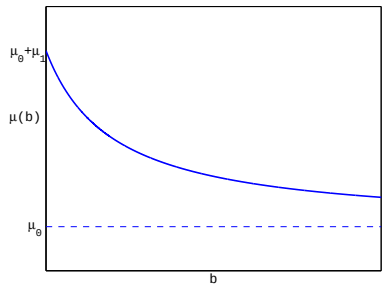

FIGURE 2. The graph of biomass per capita death rate $\mu(b) = \mu_0 + \frac{\mu_1}{b+1}$. Here $\mu_0 = 0.5$, $\mu_1 = 2$, and $0 \le b \le 10$.

When $\mu_1 = 0$ (that is, the biomass per capita death rate is a constant), system (1) is reduced to a well-known epidemic model (with some proper rescaling): SIR model with birth/death. In that context, $w(t)$ is the susceptible population, $b(t)$ is the infective population, and the removed population can be determined by the conservation of total population. The dynamics in that situation is well-known [3]. Indeed in this special case (1) has a bare-soil equilibrium $(w_0, b_0) = (R, 0)$ for all parameter values and a unique positive equilibrium $(w^+, b^+) = \left(\mu_0, \frac{R-\mu_0}{\lambda\mu_0}\right)$ if $R > \mu_0$. By using Lyapunov theory, we have the following results (detailed proof is given in subsection 2.1).

Proposition 1.1. *Consider (1) with $\mu(b)$ given by (2). Assume that $\mu_1 = 0$ and the parameters R, λ, μ_0 are all positive. Then*

1. *If $0 < R \le \mu_0$, then the bare-soil equilibrium (w_0, b_0) is globally asymptotically stable;*
2. *If $R > \mu_0$, then the positive equilibrium (w^+, b^+) is globally asymptotically stable.*

The bifurcation diagram of (1) with $\mu_1 = 0$ looks like the one in Figure 3 (a) when using the rain-fall rate R as the bifurcation parameter. Hence one can conclude that the dynamics of (1) with $\mu_1 = 0$ is a relatively simple one: when increasing

the rain-fall, there is a direct transition from the bare-soil state to the vegetation state.

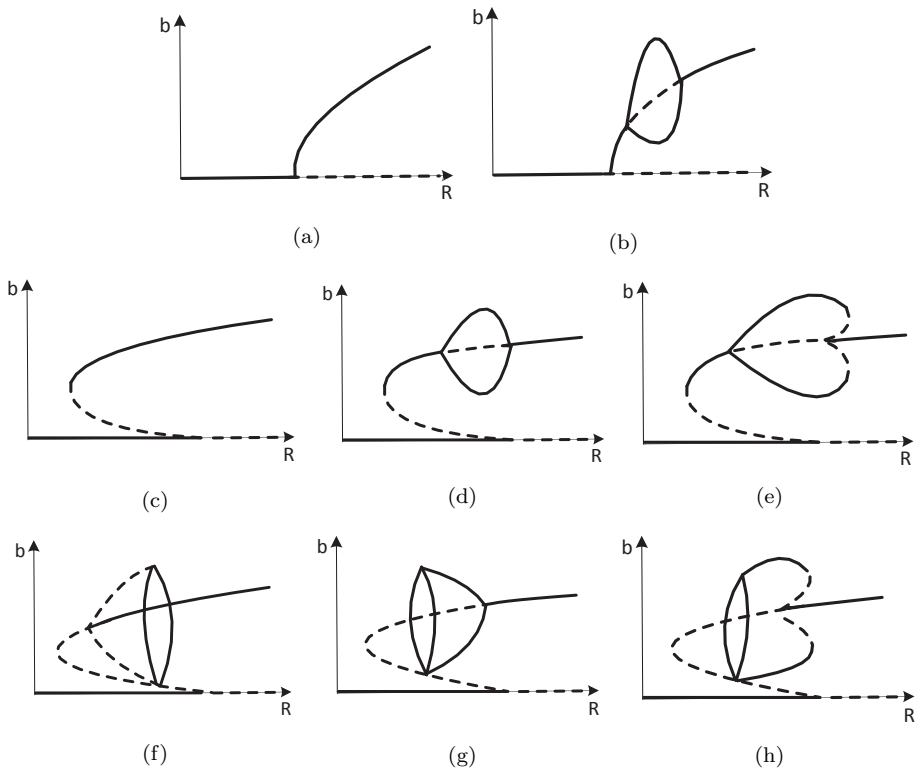

FIGURE 3. Possible bifurcation diagrams for (1)-(2) for different (λ, μ_0, μ_1). In all diagrams, the horizontal axis is the rain-fall rate R, and the vertical axis is the biomass b. (a) forward bifurcation and no cycle; (b) forward bifurcation and bubble loop of cycles; (c) backward bifurcation and no cycle; (d) backward bifurcation and bubble loop of cycles; (e) backward bifurcation, and bubble loop of cycles with one subcritical and one supercritical Hopf bifurcations and a saddle-node bifurcation of cycles; (f) backward bifurcation, subcritical Hopf bifurcation, and branch of cycles into a homoclinic bifurcation; (g) backward bifurcation, supercritical Hopf bifurcation, and branch of cycles into a homoclinic bifurcation; (h) backward bifurcation, subcritical Hopf bifurcation, saddle-node bifurcation of cycles and branch of cycles into a homoclinic bifurcation.

In this paper, we consider (1) with a decreasing biomass per capita death rate as in (2) which captures the infiltration feedback, and we show that when $\mu_1 > 0$, system (1) can exhibit surprisingly rich dynamics. While mathematical details of our result will appear in later sections, we summarize our main findings using the bifurcation diagrams in Figure 3. In all bifurcation diagrams shown in Figure 3, the horizontal axis is the rain-fall rate R, and the vertical axis is the biomass b. We use solid curve to represent stable equilibria, and dashed curve for unstable one; and we use an upper-lower pair of solid curve to represent stable periodic orbits, and dashed pair for unstable one. When $\mu_1 = 0$, a simple diagram as in Figure 3 (a)

predicts convergence to bare-soil or vegetation equilibrium. When μ_1 is positive, several complications of bifurcation diagrams can occur:

1. *Backward bifurcation of positive equilibria.* The positive equilibria emerges from the bare-soil ones through a transcritical bifurcation when increasing R. The ones in Figure 3 (a) and (b) are forward bifurcation, and the ones in (c)-(h) are backward ones. The phenomenon of backward bifurcations has been found in many epidemic models [2, 3, 9, 34], and here it occurs as a result of higher infiltration for higher biomass density.
2. *Saddle-node bifurcation of positive equilibria.* If there is a backward bifurcation of positive equilibria, note that there is no positive equilibria for small positive R, then the branch of positive equilibria necessarily turns back at a saddle-node bifurcation point for equilibria as seen in Figure 3 (c)-(h). The two equilibria for R near the bifurcation point can be a saddle and a stable node (as in (c)-(e)), but they can also be a pair of a saddle and an unstable node (as in (f)-(h)). We remark that this was also found in some other water-plant models [14].
3. *Closed loop ("bubble" or "heart") of periodic orbits.* For certain parameter range, oscillatory patterns emerge at the intermediate rain-fall rates. Indeed, we show that periodic orbits do not exist for small or large R. When there are two Hopf bifurcation points, the branch of periodic orbits form a closed loop starting and ending on the high vegetation equilibrium (Figure 3 (b), (d) and (e)). We call the ones in (b) and (d) "bubble", and the one in (e) "heart". The difference is that in (b) and (d), both Hopf bifurcations are supercritical and bifurcating limit cycles are stable, while in (e), one of Hopf bifurcations is subcritical. In the latter case, a saddle-node bifurcation of periodic orbits always occurs so the shape of the closed loop is like a heart. The bubble loop of limit cycles are more frequently found in delay differential equation models with delay as bifurcation parameter, for example [19, 29], but not so often in purely ODE models.
4. *Homoclinic orbit, homoclinic bifurcation and open ended branch ("lotus" or "pepper") of periodic orbits.* In Figure 3 (f)-(h), an unstable node merges from the saddle-node bifurcation of equilibria, and there is only one Hopf bifurcation point when increasing R. Hence the branch of periodic orbits cannot be a closed loop with two ends. Instead the other end of the branch is a homoclinic orbit in this case. This is known as a homoclinic bifurcation for which the period of limit cycles tends to infinity when approaching to the homoclinic bifurcation point. When there is no more bifurcation on the branch of cycles, we call the open ended branch of periodic orbits to be a "lotus" ((f) and (g)), and we call it a "pepper" if there is another saddle-node bifurcation of cycles on the branch (h). Note that the "lotus" can either be forward (f) or backward (g).
5. *Bogdanov-Takens bifurcation.* All bifurcation phenomena described above are codimension one with parameter R. By using R and μ_1 as bifurcation unfolding parameters, we show that a codimension two Bogdanov-Takens bifurcation (see [16]) occurs at the intersection of the Hopf bifurcation curve and the equilibrium saddle-node bifurcation curve. In this bifurcation scenario, the saddle-node bifurcation produces a saddle and unstable node, the unstable undergoes a Hopf bifurcation generating a limit cycle, and the cycle continues in the "lotus" to a homoclinic orbit based on the saddle equilibrium.

Figure 3 (f)-(h) shows several possible one-dimensional cross sections of the Bogdanov-Takens bifurcation, and see Section 4 for more details.

Compared with the simple monostable dynamics when $\mu_1 = 0$, the system (1) with (2) shows bistability of (i) two equilibria (Figure 3 (c), (d)-(f) for some R); (ii) one equilibrium and one limit cycle (Figure 3 (d)-(h) for some R), or even possibly tristability of (iii) two equilibria and one limit cycle (Figure 3 (h) for some R). Specific conditions for achieving the bifurcation diagrams in Figure 3 and bistability/tristability are given in Sections 2-4. The system also have multiple locally stable equilibria, multiple periodic orbits and homoclinic orbit. Note that various bistability also appear in predator-prey type models with Allee effect in prey growth [33], while in (1) the "prey" (water) does not have an Allee effect type growth.

The bifurcation phenomena revealed above have been documented in textbooks of dynamical systems [16], but it is rare that all of them appear in the same simple model like (1)-(2). This is perhaps a minimal model to have all these dynamical behavior of backward equilibrium transcritical bifurcation, saddle-node bifurcations for equilibria and limit cycles, Hopf bifurcations, limit cycle bubble/heart, homoclinic bifurcation, and Bogdanov-Takens bifurcation.

Our mathematical results here have interesting biological implications. In all bifurcation scenarios in Figure 3, the bare-soil equilibrium is globally asymptotically stable for low rain-fall rate R, and the higher positive vegetation equilibrium is globally asymptotically stable for high rain-fall rate R (see subsection 2.3), which is not surprising. However for intermediate rain-fall rate, many different dynamical behavior are shown in Figure 3. Note that each of Figure 3 (c)-(h) has a backward bifurcation and a hysteresis loop when R decreases. The hysteresis loop predicts a catastrophic shift from the higher vegetation state to the bare-soil state at the saddle-node bifurcation point, which has been the main feature of many studies of ecological or physical phase transitions [21, 25, 27]. Moreover the early warning sign of catastrophic shift has been a recent hot topic, as it is important to predict and prevent such catastrophic changes [4, 26]. Our results shown in Figure 3 (d)-(e) suggest that oscillatory patterns can occur at the intermediate rain-fall rate, that can be regarded as an early warning sign of getting close to the tipping point (saddle-node bifurcation point).

While the system (1) models the interaction between water and plants, it can also be interpreted as an epidemic model as mentioned earlier for the case of $\mu_1 = 0$. In that context, the term $\mu(b)b = \mu_0 b + \dfrac{\mu_1 b}{b+1}$ can be broken into two terms: $\mu_0 b$ represents moving from infected to removed class, and $\dfrac{\mu_1 b}{b+1}$ indicates the treatment of infected individuals. Similar SIR models with birth/death and treatment have been considered in [32, 34, 38, 39]. In all these work, backward bifurcation has been discovered and some also found Hopf bifurcation and existence/nonexistence of limit cycles. But none of these work considered limit cycle bubble, homoclinic bifurcation, and Bogdanov-Takens bifurcation.

This paper is organized as follows. In Section 2, we analyze the existence, local and global stability of equilibria. In Section 3, we show the occurrence of Hopf bifurcations and homoclinic bifurcations. The Bogdanov-Takens bifurcation analysis is given in Section 4. We end with some more discussions in Section 5.

2. Equilibria and stability.

2.1. **Preliminaries.** The system corresponding to (1) with death rate given in (2) is in form

$$\begin{cases} \dfrac{dw}{dt} = R - \lambda wb - w := F(w,b), \\ \dfrac{db}{dt} = wb - \left(\mu_0 + \dfrac{\mu_1}{b+1}\right) b := G(w,b), \\ w(0) \geq 0,\ b(0) > 0. \end{cases} \tag{3}$$

It is clear that $F(w,b), G(w,b)$ are analytic functions in the first quadrant $\mathbf{R}^2_+ = \{(w,b) \in \mathbf{R}^2 : w \geq 0, b \geq 0\}$. We also assume all the parameters R, λ, μ_0, μ_1 are positive. We first show that system (3) is as "well behaved" as one intuits from the biological problem.

Lemma 2.1. *Any solution of (3) is positive for $t > 0$, exists for $t \in (0, \infty)$ and is eventually bounded, i.e., let*

$$k_1 = \min\{1, \mu_0\}, \tag{4}$$

then for any $\varepsilon > 0$, there exists $T > 0$,

$$\frac{Rk_1}{R + k_1 + \varepsilon} \leq w(t) \leq R + \varepsilon, \quad \text{and} \quad 0 < b(t) \leq \frac{R+\varepsilon}{\lambda k_1} \quad \text{for } t > T. \tag{5}$$

Proof. For system (3), we have $w'|_{w=0} = R > 0$ and

$$b(t) = b(0) \exp\left(\int_0^\infty (w(s) - \mu_0 - \frac{\mu_1}{b(s)+1})ds\right) > 0.$$

So the solution is positive. Next we show the boundedness of the solution. Firstly, from the water equation we see that $\limsup_{t\to\infty} w(t) \leq R$. Then for any $\varepsilon > 0$, there exists a $T_1 > 0$ such that $w(t) \leq R + \varepsilon$ for $t > T_1$.

Let

$$k_1 = \min\{1, \mu_0\}, \quad k_2 = \max\{1, \mu_0 + \mu_1\}.$$

Then

$$R - k_2(w + \lambda b) \leq (w + \lambda b)' \leq R - k_1(w + \lambda b),$$

which yields that

$$\frac{R}{k_2} \leq \liminf_{t\to\infty}(w(t) + \lambda b(t)) \leq \limsup_{t\to\infty}(w(t) + \lambda b(t)) \leq \frac{R}{k_1}.$$

Then there exists a $T_2 > 0$ such that $b(t) \leq \dfrac{R+\varepsilon}{\lambda k_1}$ for $t > T_2$. Thus, we have

$$w'(t) \geq R - \left(\frac{R+\varepsilon}{k_1} + 1\right) w(t),$$

which yields

$$\liminf_{t\to\infty} w(t) \geq \frac{Rk_1}{R + k_1}.$$

This shows that there exists a $T_3 > 0$ such that $w(t) \geq \dfrac{Rk_1}{R + k_1 + \varepsilon}$ for $t > T_3$. Let $T = \max\{T_1, T_2, T_3\}$, we obtain (5) which also implies the global existence in time. □

The system (3) has a trivial (bare-soil) equilibrium $(w_0, b_0) = (R, 0)$ for all parameters. A positive equilibrium (w, b) satisfies

$$w = \frac{R}{\lambda b + 1}, \quad R = (\lambda b + 1)\left(\mu_0 + \frac{\mu_1}{b+1}\right). \tag{6}$$

So b is a positive root of the quadratic equation

$$\mu_0 \lambda b^2 + (\mu_0(\lambda+1) + \mu_1\lambda - R)b + \mu_0 + \mu_1 - R = 0. \tag{7}$$

Define

$$\begin{aligned} &\Delta_0 = (\mu_0(\lambda+1) + \mu_1\lambda - R)^2 - 4\lambda\mu_0(\mu_0 + \mu_1 - R), \\ &R_0 = \mu_0 + \mu_1, \quad R_1 = (\sqrt{(1-\lambda)\mu_0} + \sqrt{\lambda\mu_1})^2, \end{aligned} \tag{8}$$

and

$$b^{\pm} = b^{\pm}(R) = \frac{R - (\lambda+1)\mu_0 - \lambda\mu_1 \pm \sqrt{\Delta_0}}{2\lambda\mu_0}. \tag{9}$$

First we have the following result about the positive equilibria of (3) from elementary calculation.

Theorem 2.2. *Assume that the parameters R, λ, μ_0, μ_1 are all positive and let $\Delta_0, R_0, R_1, b^{\pm}$ be defined as in (8) and (9). Then*

1. *If either $\lambda \geq 1$ or $0 \leq \mu_1 \leq \dfrac{\lambda\mu_0}{1-\lambda}$, then the system (3) has a unique positive equilibrium $(w^+, b^+) = \left(\dfrac{R}{\lambda b^+ + 1}, b^+\right)$ when $R > R_0$, and has no positive equilibrium if $R \leq R_0$.*
2. *If $\mu_1 > \dfrac{\lambda\mu_0}{1-\lambda}$, then the system (3) has a unique positive equilibrium $(w^+, b^+) = \left(\dfrac{R}{\lambda b^+ + 1}, b^+\right)$ when $R \geq R_0$ and $R = R_1$, has two positive equilibria $(w^{\pm}, b^{\pm}) = \left(\dfrac{R}{\lambda b^{\pm} + 1}, b^{\pm}\right)$ when $R_1 < R < R_0$, and has no positive equilibrium when $R < R_1$.*

In the following (w^+, b^+) is referred as the higher vegetation state, while (w^-, b^-) is the lower vegetation state. It is useful to note that for any $b > 0$, there is at most one $R = R(b)$ such that some (w, b) is a positive equilibrium for $R = R(b)$. Indeed from (7), it is easy to solve that

$$R(b) = \frac{\mu_0\lambda b^2 + (\mu_0(\lambda+1) + \mu_1\lambda)b + \mu_0 + \mu_1}{b+1}. \tag{10}$$

Note that in the (R, b) bifurcation diagram, $R = R_1$ is a saddle-node bifurcation point and $R = R_0$ is a transcritical bifurcation point where positive equilibria bifurcate from the bare-soil equilibrium. To determine whether the bifurcation at $R = R_0$ is supercritical or subcritical for the positive equilibria, from (10) we have the slope of the positive equilibrium branch at zero biomass density:

$$R'(0) = \lambda(\mu_0 + \mu_1) - \mu_1.$$

Then the bifurcation at $R = R_0$ is subcritical (backward) if

$$0 < \lambda < 1 \quad \text{and} \quad \mu_1 > \frac{\lambda\mu_0}{1-\lambda}, \tag{11}$$

and it is supercritical (forward) if

$$0 < \lambda < 1 \quad \text{and} \quad 0 \le \mu_1 \le \frac{\lambda\mu_0}{1-\lambda}, \quad \text{or} \quad \lambda \ge 1. \tag{12}$$

See Figure 3 (a)-(b) for illustration of forward bifurcations, and Figure 3 (c)-(h) for backward ones.

We end this subsection with a proof of Proposition 1.1.

Proof of Proposition 1.1. For part 1, we use a Lyapunov function

$$E_1(w,b) := w - w_0 - w_0 \ln \frac{w}{w_0} + \lambda b. \tag{13}$$

Its derivative along the solutions of (1) is

$$\begin{aligned}\dot{E}_1(w(t),b(t)) &= \left(1 - \frac{w_0}{w}\right)(R - \lambda w b - w) + \lambda b\,(w - \mu_0)\\ &= -R\left(\frac{w}{w_0} + \frac{w_0}{w} - 2\right) + \lambda(R - \mu_0)b.\end{aligned}$$

Note that $\frac{w}{w_0} + \frac{w_0}{w} - 2 \ge 0$. Thus, $\dot{E}_1 \le 0$ if $R \le \mu_0$ and $\dot{E}_1 = 0$ only if $(w(t), b(t)) = (R, 0)$. Hence, from LaSalle's invariance principle, all solutions ultimately approach the bare-soil equilibrium (w_0, b_0) if $0 < R \le \mu_0$.

For part 2, we use a Lyapunov function

$$E_2(w,b) := w - w^+ - w^+ \ln \frac{w}{w^+} + \lambda\left(b - b^+ - b^+ \ln \frac{b}{b^+}\right). \tag{14}$$

Using the fact that $R = \lambda w^+ b^+ + w^+$ and $\frac{w}{w^+} + \frac{w^+}{w} - 2 \ge 0$, we have

$$\begin{aligned}\dot{E}_2(w(t),b(t)) &= \left(1 - \frac{w^+}{w}\right)(R - \lambda w b - w) + \lambda(b - b^+)(w - \mu_0)\\ &= -w^+\left(\frac{w}{w^+} + \frac{w^+}{w} - 2\right) - \lambda w^+ b^+\left(\frac{w}{w^+} + \frac{w^+}{w} - 2\right)\\ &= -w^+(1 + \lambda b^+)\left(\frac{w}{w^+} + \frac{w^+}{w} - 2\right) \le 0.\end{aligned}$$

Furthermore, $\dot{E}_2 = 0$ only if $(w(t), b(t)) = (w^+, b^+)$ or $(w(t), b(t)) = (R, 0)$. Note that $(R, 0)$ is unstable when $R > \mu_0$. Then from LaSalle's invariance principle, the positive equilibrium (w^+, b^+) is globally asymptotically stable for all nonnegative initial values except $(R, 0)$ whenever it exists. □

Remark 2.3. When $\mu_1 = 0$, the model considered in Proposition 1.1 is the same as (after a rescaling) the classical SIR epidemic model with birth/death: (here $a, \alpha, \beta > 0$)

$$\begin{cases} \dfrac{dS}{dt} = a - \alpha SI - aS, \\ \dfrac{dI}{dt} = \alpha SI - \beta I - aI, \\ \dfrac{dR}{dt} = \beta I - aR, \end{cases} \tag{15}$$

with basic reproduction number $\mathcal{R}_0 = \beta/\alpha$. In (15), $S(t), I(t)$ and $R(t)$ denote the number of individuals that are susceptible to infection, that are infectious, and that have been removed with immunity, respectively. The parameter a is the birth (death) rate, α is the incidence rate and β is the natural recovery rate of the infective

individuals. Clearly (1) with $\mu_1 = 0$ is equivalent to the first two equations of (15) with a "basic reproduction number" $\mathcal{R}_0 = R/\mu_0$. We shall return to the discussion of connection between (1) (with $\mu_1 > 0$) and epidemic models in Section 5.

2.2. **Local stability of equilibria.** From Theorem 2.2, the system (3) may have three non-negative equilibria: $(R, 0)$, (w^-, b^-) and (w^+, b^+). In this subsection we investigate the local stability of these equilibria. First we have the following results for the equilibria $(R, 0)$ and (w^-, b^-).

Proposition 2.4. *Assume that the parameters R, λ, μ_0, μ_1 are all positive. Then*

1. *The bare-soil equilibrium $(R, 0)$ is locally asymptotically stable when $R < R_0$, and it is unstable when $R > R_0$, where R_0 is defined in (8).*
2. *The positive equilibrium (w^-, b^-) is an unstable saddle whenever it exists.*

Proof. The associated Jacobian matrix at an equilibrium (w, b) is given by

$$J(w,b) = \begin{pmatrix} -\lambda b - 1 & -\lambda w \\ b & w - \mu_0 - \dfrac{\mu_1}{(b+1)^2} \end{pmatrix}.$$

Then at the bare-soil equilibrium $(w_0, b_0) = (R, 0)$,

$$J(R,0) = \begin{pmatrix} -1 & 0 \\ 0 & R - (\mu_0 + \mu_1) \end{pmatrix},$$

which shows that $(R, 0)$ is locally asymptotically stable when $R < R_0$, and it is unstable when $R > R_0$.

At the equilibrium (w^-, b^-), the associated Jacobian matrix is

$$J(w^-,b^-) = \begin{pmatrix} -\lambda b^- - 1 & -\dfrac{\lambda R}{\lambda b^- + 1} \\ b^- & \dfrac{\mu_1 b^-}{(b^-+1)^2} \end{pmatrix}.$$

Then

$$\begin{aligned} \mathrm{Det}(J(w^-,b^-)) &= \frac{\lambda R b^-}{\lambda b^- + 1} - (\lambda b^- + 1)\frac{\mu_1 b^-}{(b^-+1)^2} \\ &= b^- \left[\lambda \left(\mu_0 + \frac{\mu_1}{b^- + 1} \right) - \frac{\mu_1(\lambda b^- + 1)}{(b^-+1)^2} \right]. \end{aligned}$$

On the other hand, by using (10), a direct calculation shows that

$$R'(b) = \lambda \left(\mu_0 + \frac{\mu_1}{b+1} \right) - \frac{\mu_1(\lambda b + 1)}{(b+1)^2}. \tag{16}$$

Thus we have $\mathrm{Det}(J(w^-, b^-)) = b^- R'(b^-)$. Furthermore, from (16) we have

$$R'(b) = \frac{1}{(b+1)^2} \left[\lambda\mu_0 b^2 + 2\lambda\mu_0 b + \lambda(\mu_0 + \mu_1) - \mu_1 \right]. \tag{17}$$

If (w^-, b^-) exists, we have $\mu_1 > \dfrac{\lambda\mu_0}{1-\lambda}$ and $b^- < b(R_1)$ which imply that $R'(b^-) < 0$, where R_1 is the saddle-node bifurcation point defined in (8) and $b(R_1) = \dfrac{\sqrt{\lambda(1-\lambda)\mu_0\mu_1} - \lambda\mu_0}{\lambda\mu_0}$. Thus we have $\mathrm{Det}(J(w^-, b^-)) < 0$ which shows that (w^-, b^-) is always a saddle equilibrium. □

Next we discuss the local stability of (w^+, b^+). We consider the two cases that λ satisfies $0 < \lambda < 1$ and $\lambda \geq 1$ separately. For the case of $0 < \lambda < 1$, we define

$$m(\mu_0) = \frac{\mu_0}{\lambda(1-\lambda)} \left(\lambda + \frac{1-\lambda}{\mu_0 - (1-\lambda)} \right)^2, \quad \text{for } \mu_0 > 1 - \lambda, \tag{18}$$

and

$$\begin{aligned} \mu_0^*(\lambda) &= \frac{(1-\lambda)(2\lambda + 1 + \sqrt{8\lambda+1})}{2\lambda}, \\ \mu_1^*(\lambda) &= \frac{(4\lambda + 5 + 3\sqrt{8\lambda+1})(4\lambda - 1 + \sqrt{8\lambda+1})}{16\lambda}, \\ \mu_0^{**}(\lambda) &= \frac{(1-\lambda)\mu_1^*(\lambda)}{\lambda}. \end{aligned} \tag{19}$$

Define the subregions I, II, III, IV and V in the $\mu_0 - \mu_1$ plane as follows (see Figure

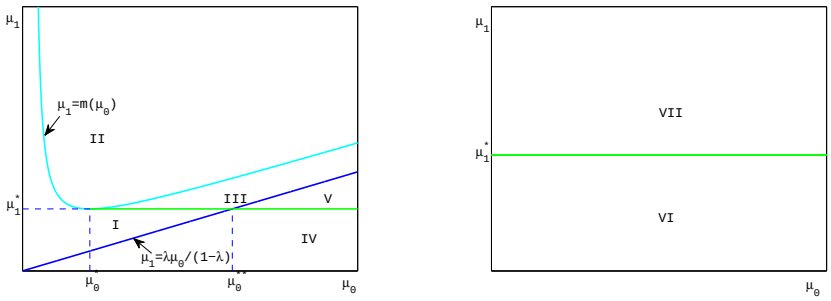

FIGURE 4. Illustration of the stability parameter subregions in the $\mu_0 - \mu_1$ plane. (Left) $0 < \lambda < 1$; (Right) $\lambda \geq 1$.

4 left panel):

$$\mathrm{I} = \mathrm{I}_1 \bigcup \mathrm{I}_2, \tag{20}$$

where

$$\begin{aligned} \mathrm{I}_1 &= \left\{ (\mu_0, \mu_1) : 0 < \mu_0 \leq 1 - \lambda, \mu_1 > \frac{\lambda \mu_0}{1-\lambda} \right\} \\ &\quad \bigcup \left\{ (\mu_0, \mu_1) : 1 - \lambda < \mu_0 < \mu_0^*, \frac{\lambda \mu_0}{1-\lambda} < \mu_1 < m(\mu_0) \right\}, \\ \mathrm{I}_2 &= \left\{ (\mu_0, \mu_1) : \mu_0^* < \mu_0 < \mu_0^{**}, \frac{\lambda \mu_0}{1-\lambda} < \mu_1 < \mu_1^* \right\}; \end{aligned} \tag{21}$$

and

$$\begin{aligned} \mathrm{II} &= \{ (\mu_0, \mu_1) : \mu_0 > 0, \mu_1 > m(\mu_0) \}; \\ \mathrm{III} &= \left\{ (\mu_0, \mu_1) : \mu_0 > \mu_0^*, \max \left\{ \mu_1^*, \frac{\lambda \mu_0}{1-\lambda} \right\} < \mu_1 < m(\mu_0) \right\}; \\ \mathrm{IV} &= \left\{ (\mu_0, \mu_1) : \mu_0 > 0, 0 < \mu_1 < \min \left\{ \frac{\lambda \mu_0}{1-\lambda}, \mu_1^* \right\} \right\}; \\ \mathrm{V} &= \left\{ (\mu_0, \mu_1) : \mu_0 > \mu_0^{**}, \mu_1^* < \mu_1 < \frac{\lambda \mu_0}{1-\lambda} \right\}. \end{aligned} \tag{22}$$

Then the local stability of (w^+, b^+) is as follows:

Theorem 2.5. *Assume that the parameters R, λ, μ_0, μ_1 are all positive and $0 < \lambda < 1$. Let $m(\mu_0), \mu_0^*, \mu_1^*, \mu_0^{**}$ and subregions I, II, III, IV and V be defined as above.*

1. *If $(\mu_0, \mu_1) \in I \bigcup IV$, then (w^+, b^+) is locally asymptotically stable;*
2. *If $(\mu_0, \mu_1) \in II$, then there exists R_3 with $R_3 > R_1$ such that (w^+, b^+) is unstable when $R_1 < R < R_3$, and it is locally asymptotically stable when $R > R_3$;*
3. *If $(\mu_0, \mu_1) \in III \bigcup V$, then there exist R_2, R_3 with $R_1 < R_2 < R_3$ such that (w^+, b^+) is unstable when $R_2 < R < R_3$, and it is locally asymptotically stable when $R_1 < R < R_2$ or $R > R_3$.*

On the other hand, for the case that $\lambda \geq 1$, we define the subregions VI, VII in $\mu_0 - \mu_1$ plane (see Figure 4 right panel):

$$\begin{aligned} \text{VI} &= \{(\mu_0, \mu_1) : 0 < \mu_1 \leq \mu_1^*(\lambda)\}; \\ \text{VII} &= \{(\mu_0, \mu_1) : \mu_1 > \mu_1^*(\lambda)\}. \end{aligned} \tag{23}$$

Then the local stability of (w^+, b^+) is as follows:

Theorem 2.6. *Assume that the parameters R, λ, μ_0, μ_1 are all positive and $\lambda \geq 1$. Let μ_1^* be defined as (19) and VI, VII be defined as in (23). Then we have*

1. *If $(\mu_0, \mu_1) \in VI$, then (w^+, b^+) is locally asymptotically stable;*
2. *If $(\mu_0, \mu_1) \in VII$, then there exist R_2, R_3 with $R_0 < R_2 < R_3$ such that (w^+, b^+) is unstable when $R_2 < R < R_3$, and it is locally asymptotically stable when $R_0 < R < R_2$ or $R > R_3$.*

The proofs of Theorems 2.5 and 2.6 are technical, and we postpone them to subsection 2.4.

2.3. **Global stability and nonexistence of periodic orbits.** In this subsection, we discuss the global dynamical behavior of the system (3). First of all, the bare-soil equilibrium is globally asymptotically stable if the rain-fall rate R is low. More precisely, we have

Proposition 2.7. *Assume that the parameters R, λ, μ_0, μ_1 are all positive and let k_1 be defined as (4). If*

$$0 \leq R < \frac{\mu_0 - \lambda k_1 + \sqrt{(\lambda k_1 + \mu_0)^2 + 4\lambda k_1 \mu_1}}{2} \equiv R_{**}, \tag{24}$$

then $(R, 0)$ is globally asymptotically stable for system (3).

Proof. According to Lemma 2.1, for any $\varepsilon > 0$, there exists a $T_1 > 0$ such that $0 < b(t) \leq \dfrac{R + \varepsilon}{\lambda k_1}$ for $t > T_1$, where k_1 is defined as (4). Then, for system (3), we have

$$b'(t) \leq b(t)\left(R - \mu_0 - \frac{\mu_1}{b(t) + 1}\right) \leq b(t)\left(R - \mu_0 - \frac{\mu_1}{(R + \varepsilon)/(\lambda k_1) + 1}\right) \tag{25}$$

for $t > T_1$. So, if $0 \leq R < \mu_0 + \dfrac{\lambda \mu_1 k_1}{R + \lambda k_1}$, *i.e.* R satisfies (24), we have $\lim\limits_{t \to \infty} b(t) = 0$. Thus there exists a T_2 such that $b(t) < \varepsilon$ for $t > T_2$, and

$$R - (1 + \lambda\varepsilon) w(t) \leq w'(t) \leq R - w(t). \tag{26}$$

This clearly shows that $\lim\limits_{t \to \infty} w(t) = R$. □

Our next result is that when the rain-fall rate R is either low or high, the system (3) cannot have a periodic orbit. Define

$$R_* = \mu_0 + 1, \qquad R^* = \mu_1(1 + \lambda + \mu_0), \tag{27}$$

Then by the Dulac criterion we can eliminate the possibility of periodic orbits in the system (3) in the following result for low or high rain-fall rate R.

Proposition 2.8. *Assume that the parameters R, λ, μ_0, μ_1 are all positive and let R_* and R^* be defined as in (27). Then for $0 < R \le R_*$ or $R \ge R^*$, system (3) has no periodic orbits.*

Proof. We prove by using the Dulac Criterion. Define a Dulac function in the form (see [10, 11])

$$D(w, b) = s(w)r(b),$$

where $s(w)$ and $r(b)$ are to be determined later. Then along solution orbits of system (3), we have

$$\begin{aligned}\frac{\partial(FD)}{\partial w} + \frac{\partial(GD)}{\partial b} &= D(w,b)\left(\frac{\partial F}{\partial w} + \frac{\partial G}{\partial b} + F\frac{s'(w)}{s(w)} + G\frac{r'(b)}{r(b)}\right)\\ &= D(w,b)\left[-1 - \mu_0 - \lambda b - \frac{\mu_1}{(b+1)^2} - (\mu_0 + \frac{\mu_1}{b+1})b\frac{r'(b)}{r(b)}\right.\\ &\qquad \left. + w + (R - w - \lambda w b)\frac{s'(w)}{s(w)} + wb\frac{r'(b)}{r(b)}\right].\end{aligned} \tag{28}$$

Let $s(w) = e^{cw}$ where c is a constant to be determined. Then $s'(w)/s(w) = c$ and (28) is reduced to

$$\begin{aligned}\frac{\partial(FD)}{\partial w} + \frac{\partial(GD)}{\partial b} &= D(w,b)\left[Rc - 1 - \mu_0 - \lambda b - \frac{\mu_1}{(b+1)^2} - (\mu_0 + \frac{\mu_1}{b+1})b\frac{r'(b)}{r(b)}\right.\\ &\qquad \left. + w\left(1 - c - \lambda cb + b\frac{r'(b)}{r(b)}\right)\right].\end{aligned} \tag{29}$$

In (29), we choose $r(b) = e^{\lambda cb}b^{c-1}$ so that $r(b)$ satisfies

$$1 - c - \lambda cb + b\frac{r'(b)}{r(b)} = 0, \tag{30}$$

From (29) and (30), it follows that

$$\begin{aligned}&\frac{\partial(FD)}{\partial w} + \frac{\partial(GD)}{\partial b}\\ &= D(w,b)\left[Rc - 1 - \mu_0 - \lambda b - \frac{\mu_1}{(b+1)^2} - (\mu_0 + \frac{\mu_1}{b+1})(\lambda cb + c - 1)\right]\\ &\equiv D(w,b)H(b).\end{aligned} \tag{31}$$

Now we choose $c = 1$. Then

$$\begin{aligned}H(b) &= Rc - 1 - \mu_0 - \lambda b - \frac{\mu_1}{(b+1)^2} - (\mu_0 + \frac{\mu_1}{b+1})(\lambda cb + c - 1)\\ &= R - 1 - \mu_0 - \lambda b(1 + \mu_0) - \frac{\mu_1}{(b+1)^2} - \frac{\lambda\mu_1 b}{b+1}\\ &\le R - 1 - \mu_0,\end{aligned} \tag{32}$$

which is negative if $R \le R_* = 1+\mu_0$. Thus from Dulac Criterion, there are no nontrivial periodic solutions if $0 < R \le R_*$ and this completes the proof for the case of $0 < R \le R_*$.

For $R \ge R^*$, we choose $c = -1/\mu_0$. Then

$$\begin{aligned} H(b) &\le Rc - (1+\lambda b)(1+\mu_0 c) - \frac{\mu_1(c-1)+\lambda\mu_1 cb}{b+1} \\ &= -\frac{R}{\mu_0} + \frac{\mu_1(1+\mu_0^{-1})}{b+1} + \frac{\lambda\mu_1 b}{\mu_0(b+1)} \le -\frac{R}{\mu_0} + \mu_1\left(1+\frac{1}{\mu_0}\right) + \frac{\lambda\mu_1}{\mu_0}, \end{aligned} \tag{33}$$

which is negative if $R \ge R^* = \mu_1(1+\lambda+\mu_0)$. Hence, there are no nontrivial periodic orbits for (3) if $0 < R \le R_*$ or $R \ge R^*$. □

Combining with the existence and local stability of equilibria proved in Theorems 2.2, 2.5 and 2.6, and the classical Poincaré-Bendixon theorem for the planar systems, we obtain the following results regarding the global dynamic behavior of (3):

Theorem 2.9. *Assume that the parameters R, λ, μ_0, μ_1 are all positive. Let R_0, R_1, R_{**}, R_* and R^* be defined as in (8), (24) and (27) respectively.*

1. *When $0 < R < R_{**}$, the bail-soil equilibrium $(R, 0)$ is globally asymptotically stable, and when $R > max\{R_0, R^*\}$, the positive equilibrium (w^+, b^+) is globally asymptotically stable for system (3);*
2. *Suppose that one of the following conditions hold*

$$\lambda \ge 1 \ \text{ and } \ 0 \le \mu_1 \le \frac{1+\mu_0}{1+\mu_0+\lambda}, \tag{34}$$

or

$$0 \le \lambda < 1 \ \text{ and } \ 0 \le \mu_1 \le min\left\{\frac{1+\mu_0}{1+\mu_0+\lambda}, \frac{\lambda\mu_0}{1-\lambda}\right\}. \tag{35}$$

Then for system (3), when $0 < R \le R_0$, the bail-soil equilibrium $(R, 0)$ is globally asymptotically stable, and when $R > R_0$, the positive equilibrium (w^+, b^+) is globally asymptotically stable;

3. *Suppose that*

$$0 \le \lambda < 1 \ \text{ and } \ \frac{\lambda\mu_0}{1-\lambda} < \mu_1 \le \frac{1+\mu_0}{1+\mu_0+\lambda}. \tag{36}$$

Then for system (3), when $0 < R < R_1$, the bail-soil equilibrium $(R, 0)$ is globally asymptotically stable; when $R > R_0$, the positive equilibrium (w^+, b^+) is globally asymptotically stable; and when $R_1 < R < R_0$, then each solution of (3) tends to $(R, 0)$ or (w^+, b^+) as $t \to \infty$ except the one-dimensional stable manifold of (w^-, b^-).

Proof. Part 1 follows from Propositions 2.4, 2.8 and Poincaré-Bendixon theorem. For parts 2 and 3, we notice that if $0 \le \mu_1 \le \dfrac{1+\mu_0}{1+\mu_0+\lambda}$, then $R_* \ge R^*$. Hence system (3) has no periodic orbits for any $R > 0$. Then the results in parts 2 and 3 follow from Theorems 2.2, 2.5, 2.6 and Poincaré-Bendixon theorem. □

Theorem 2.9 show that when μ_1 is small, then the dynamics of system (3) is dominated by equilibria. That is, any solution orbit tends to a non-negative equilibrium. When μ_1 is near 0 (satisfying (34) or (35)), the dynamics of (3) has a transition from the unique vegetation equilibrium to the bare-soil state as the rainfall rate R decreases across R_0. The transition is a gradual one as the bifurcation is forward at $R = R_0$. When μ_1 is in an intermediate range (satisfying (36)), there is a

bistable parameter regime $R_1 < R < R_0$, and there is a sudden transition from high vegetation equilibrium (w^+, b^+) to the bar-soil one at $R = R_1$. Hence a hysteresis effect occurs in this case. In all these parameter ranges for μ_1, there is no limit cycle for (3), and the biomass always tends to an equilibrium level asymptotically. However as shown in Theorems 2.5 and 2.6, when μ_1 is larger, the system (3) can have oscillatory patterns for intermediate rain-fall rates. This will be shown in the Section 3.

2.4. **Proof of Theorems 2.5 and 2.6.** In this subsection we prove Theorems 2.5 and 2.6. Recall the function in (6):

$$R(b) = (\lambda b + 1)\left(\mu_0 + \frac{\mu_1}{b+1}\right).$$

With a change of variable $B = b + 1$, we see that $R(b) = \tilde{R}(B)$ where

$$\tilde{R}(B) = \lambda\mu_0 B + \frac{(1-\lambda)\mu_1}{B} + (1-\lambda)\mu_0 + \lambda\mu_1.$$

The properties of function $\tilde{R}(B)$ can be summarized as follows:

1. If $\lambda \geq 1$, then $\tilde{R}'(B) > 0$ for all $B \in (0, \infty)$;
2. If $0 < \lambda < 1$, then $\tilde{R}(B)$ has an unique critical point at $B = B_* = \sqrt{\dfrac{(1-\lambda)\mu_1}{\lambda\mu_0}}$ which is a global minimum point, and $R_1 = \tilde{R}(B_*) = (\sqrt{(1-\lambda)\mu_0} + \sqrt{\lambda\mu_1})^2$; $\tilde{R}'(B) < 0$ for $B \in (0, B_*)$ and $\tilde{R}'(B) > 0$ for $B \in (B_*, \infty)$; $\lim\limits_{B\to 0^+} \tilde{R}(B) = \lim\limits_{B\to\infty} \tilde{R}(B) = \infty$.

Let $B^+ = b^+ + 1$ then $B^+ > 1$ and we always have $\tilde{R}'(B^+) > 0$.

The associated Jacobian matrix at the equilibrium (w^+, b^+) is given by

$$J(w^+, b^+) = \begin{pmatrix} -\lambda b^+ - 1 & -\dfrac{\lambda R}{\lambda b^+ + 1} \\ b^+ & \dfrac{\mu_1 b^+}{(b^+ + 1)^2} \end{pmatrix}.$$

Then we have

$$\begin{aligned} \mathrm{Det}(J(w^+, b^+)) &= \frac{\lambda R b^+}{\lambda b^+ + 1} - (\lambda b^+ + 1)\frac{\mu_1 b^+}{(b^+ + 1)^2} \\ &= b^+\left[\lambda(\mu_0 + \frac{\mu_1}{b^+ + 1}) - (\lambda b^+ + 1)\frac{\mu_1}{(b^+ + 1)^2}\right] \\ &= (B^+ - 1)\tilde{R}'(B^+) > 0. \end{aligned}$$

And the trace of $J(w^+, b^+)$ is given by

$$\mathrm{Trace}(J(w^+, b^+)) = \frac{1}{(b^+ + 1)^2}\left[\mu_1 b^+ - (\lambda b^+ + 1)(b^+ + 1)^2\right]$$

where $b^+ = b^+(R)$ is defined as in (9).

Let

$$f(b) = \mu_1 b - (\lambda b + 1)(b + 1)^2.$$

Then $f(b) = \tilde{f}(B)$, where

$$\tilde{f}(B) = -\lambda B^3 + (\lambda - 1)B^2 + \mu_1 B - \mu_1. \tag{37}$$

We consider the sign of $f(b)$ for $b = b^+$, or equivalently the one for $\tilde{f}(B)$ for $B = B^+$. The properties of function $\tilde{f}(B)$ can be summarized as follows:

1. $\tilde{f}(B)$ has at most two zeros in $(0,\infty)$, since $\lim_{B\to-\infty} \tilde{f}(B) = \infty$ and $\tilde{f}(0) = -\mu_1$ then $\tilde{f}(B)$ has at least one zero in $(-\infty, 0)$;
2. From $\tilde{f}'(B) = -3\lambda B^2 + 2(\lambda-1)B + \mu_1 = 0$, we get $B = \frac{\lambda - 1 \pm \sqrt{(\lambda-1)^2 + 3\lambda\mu_1}}{3\lambda}$. Let
$$B_{**} = \frac{\lambda - 1 + \sqrt{(\lambda-1)^2 + 3\lambda\mu_1}}{3\lambda} > 0. \tag{38}$$
Then $\tilde{f}'(B_{**}) = 0$ and $\tilde{f}''(B_{**}) < 0$. So $B = B_{**}$ is a local maximum point of $\tilde{f}(B)$, and it is the unique critical point of $\tilde{f}(B)$ in $(0,\infty)$.

We consider $\tilde{f}(B)$ for two cases: $B_* > 1$ or $B_* \le 1$. For the case of $B_* > 1$, we consider $\tilde{f}(B)$ for $B \in [B_*, \infty)$, and we have the following results:

Lemma 2.10. *Assume that B, B_*, B_{**} and $\tilde{f}(B)$ are defined as above and $B_* > 1$. Then*

1. *If $B_* \ge B_{**}$ and $\tilde{f}(B_*) \le 0$, then $\tilde{f}(B) < 0$ for all $B > B_*$;*
2. *If $B_* < B_{**}$, $\tilde{f}(B_*) < 0$ and $\tilde{f}(B_{**}) > 0$, then there exist $B_2 < B_{**} < B_3$ such that $\tilde{f}(B) < 0$ for $B \in (B_*, B_2)\bigcup(B_3,\infty)$ and $\tilde{f}(B) > 0$ for $B \in (B_2, B_3)$;*
3. *If $B_* < B_{**}$ and $\tilde{f}(B_{**}) \le 0$, then $\tilde{f}(B) < 0$ for all $B > B_*$;*
4. *If $\tilde{f}(B_*) > 0$, then exists $B_3 > B_{**}$ such that $\tilde{f}(B) > 0$ for $B \in (B_*, B_3)$ and $\tilde{f}(B) > 0$ for $B \in (B_3, \infty)$.*

And for the case of $B_* \le 1$, we consider $\tilde{f}(B)$ for $B \in [1,\infty)$. Notice that $\tilde{f}(1) = -1 < 0$. Then we have the following results:

Lemma 2.11. *Assume that B_{**} and $\tilde{f}(B)$ are defined as above and $B_* \le 1$. Then*

1. *If $B_{**} < 1$, then $\tilde{f}(B) < 0$ for $B \in [1,\infty)$;*
2. *If $B_{**} > 1, \tilde{f}(B_{**}) < 0$, then $\tilde{f}(B) < 0$ for $B \in [1,\infty)$;*
3. *If $B_{**} > 1, \tilde{f}(B_{**}) > 0$, then there exist $1 < B_2 < B_{**} < B_3$ such that $\tilde{f}(B) < 0$ for $B \in [1, B_2)\bigcup(B_3,\infty)$ and $\tilde{f}(B) > 0$ for $B \in (B_2, B_3)$.*

The proofs of Lemmas 2.10 and 2.11 are elementary and we omit them here. Now we determine the ranges of parameters (λ, μ_0, μ_1) so that the conditions in Lemmas 2.10 and 2.11 are met. Define
$$m_0(\mu_0) = \frac{4\mu_0(1-\lambda)^3}{\lambda(\mu_0 - 3(1-\lambda))^2}, \quad \text{for } \mu_0 > 3(1-\lambda) \tag{39}$$
and $m(\mu_0)$ as in (18). Then we have the following results:

Lemma 2.12. *Let $B, B_*, B_{**}, \tilde{f}(B), m_0(\mu_0)$ be defined as above, let $m(\mu_0)$ be defined as in (18) and let $\mu_1^*(\lambda)$ be defined as in (19). Then*

1. *$B_* > 1$ if and only if $\mu_1 > \frac{\lambda\mu_0}{1-\lambda}$;*
2. *$B_{**} < 1$ if and only if $\mu_1 < \lambda + 2$;*
3. *If $\mu_0 \le 3(1-\lambda)$, then $B_* > B_{**}$; If $\mu_0 > 3(1-\lambda)$, then $B_* < B_{**}$ if and only if $\mu_1 > m_0(\mu_0)$;*
4. *If $\mu_0 \le 1-\lambda$, then $\tilde{f}(B_*) < 0$; If $\mu_0 > 1-\lambda$, then $\tilde{f}(B_*) < 0$ if and only if $\mu_1 < m(\mu_0)$;*
5. *$\tilde{f}(B_{**}) < 0$ if and only if $\mu_1 < \mu_1^*(\lambda)$.*

Proof. The proof of part 1 and part 2 can be easily obtained by the expressions of B_* and B_{**}. For part 3, we have

$$\begin{aligned} B_* - B_{**} &= \sqrt{\frac{(1-\lambda)\mu_1}{\lambda\mu_0}} - \frac{\lambda - 1 + \sqrt{(\lambda-1)^2 + 3\lambda\mu_1}}{3\lambda} \\ &= \frac{1}{3\lambda\mu_0}\left[3\sqrt{\lambda(1-\lambda)\mu_0\mu_1} + (1-\lambda)\mu_0 - \mu_0\sqrt{(1-\lambda)^2+3\lambda\mu_1}\right]. \end{aligned}$$

Denote $A_1 = 3\sqrt{\lambda(1-\lambda)\mu_0\mu_1} + (1-\lambda)\mu_0$ and $A_2 = \mu_0\sqrt{(1-\lambda)^2+3\lambda\mu_1}$. Then

$$A_1^2 - A_2^2 = 3\mu_0\left[\lambda(3(1-\lambda)-\mu_0)\sqrt{\mu_1} + 2(1-\lambda)\sqrt{\lambda(1-\lambda)\mu_0}\right].$$

If $\mu_0 \le 3(1-\lambda)$, then $A_1 > A_2$ which results in $B_* > B_{**}$. If $\mu_0 > 3(1-\lambda)$, then $A_1 = A_2$ when $\mu_1 = m_0(\mu_0)$, $A_1 > A_2$ when $\mu_1 < m_0(\mu_0)$, and $A_1 < A_2$ when $\mu_1 > m_0(\mu_0)$. Or equivalently $B_* = B_{**}$ when $\mu_1 = m_0(\mu_0)$, $B_* > B_{**}$ when $\mu_1 < m_0(\mu_0)$, and $B_* < B_{**}$ when $\mu_1 > m_0(\mu_0)$.

For part 4, we have

$$\begin{aligned} \tilde{f}(B_*) &= -\lambda B_*^3 + (\lambda-1)B_*^2 + \mu_1 B_* - \mu_1 \\ &= \frac{\mu_1}{\lambda\mu_0^2}\left[-(\lambda\mu_0^2 + (1-\lambda)^2\mu_0) + (\mu_0 - (1-\lambda))\sqrt{\lambda(1-\lambda)\mu_0\mu_1}\right]. \end{aligned}$$

If $\mu_0 \le 1-\lambda$, we have $\tilde{f}(B_*) < 0$. If $\mu_0 > 1-\lambda$, defining the function $m(\mu_0)$ as in (18), then we have $\tilde{f}(B_*) = 0$ when $\mu_1 = m(\mu_0)$, and $\tilde{f}(B_*) < 0$ when $\mu_1 < m(\mu_0)$; $\tilde{f}(B_*) > 0$ when $\mu_1 > m(\mu_0)$.

To prove part 5, from the equation $\tilde{f}'(B_{**}) = 0$ we have $\mu_1 = 3\lambda B_{**}^2 - 2(\lambda-1)B_{**}$. Then

$$\begin{aligned} \tilde{f}(B_{**}) &= -\lambda B_{**}^3 + (\lambda-1)B_{**}^2 + \mu_1 B_{**} - \mu_1 \\ &= -\lambda B_{**}^3 + (\lambda-1)B_{**}^2 + (B_{**}-1)[3\lambda B_{**}^2 - 2(\lambda-1)B_{**}] \\ &= B_{**}[2\lambda B_{**}^2 + (1-4\lambda)B_{**} + 2(\lambda-1)]. \end{aligned}$$

Hence $\tilde{f}(B_{**}) > 0$ when $B_{**} > \tilde{B}$, and $\tilde{f}(B_{**}) < 0$ when $B_{**} < \tilde{B}$, where $\tilde{B} = \dfrac{4\lambda - 1 + \sqrt{1+8\lambda}}{4\lambda}$. Notice that

$$\begin{aligned} B_{**} - \tilde{B} &= \frac{\lambda - 1 + \sqrt{(\lambda-1)^2+3\lambda\mu_1}}{3\lambda} - \frac{4\lambda - 1 + \sqrt{1+8\lambda}}{4\lambda} \\ &= \frac{1}{3\lambda}\left[\sqrt{(1-\lambda)^2+3\lambda\mu_1} - \left(2\lambda + 1 + \frac{-3+3\sqrt{1+8\lambda}}{4}\right)\right]. \end{aligned}$$

Define $\mu_1^*(\lambda)$ as in (19). Then we have $B_{**} = \tilde{B}$ if $\mu_1 = \mu_1^*(\lambda)$; $B_{**} > \tilde{B}$ if $\mu_1 > \mu_1^*(\lambda)$; and $B_{**} < \tilde{B}$ if $\mu_1 < \mu_1^*(\lambda)$. Thus we have $\tilde{f}(B_{**}) < 0$ when $\mu_1 < \mu_1^*(\lambda)$; $\tilde{f}(B_{**}) > 0$ when $\mu_1 > \mu_1^*(\lambda)$. □

To prove Theorem 2.5, we point out some properties of the functions $\mu_1 = m_0(\mu_0)$ and $\mu_1 = m(\mu_0)$.

1. The function $\mu_1 = m_0(\mu_0)$, with $\mu_0 = 3(1-\lambda)$ as the vertical asymptote and $\mu_1 = 0$ as the oblique asymptote, is decreasing in the interval $(3(1-\lambda), +\infty)$ and intersects with the line $\mu_1 = \dfrac{\lambda\mu_0}{1-\lambda}$ at a certain point $((1-\lambda)(\lambda+2)/\lambda, \lambda+2)$.

2. The function $\mu_1 = m(\mu_0)$, with $\mu_0 = 1-\lambda$ as the vertical asymptote and $\mu_1 = \frac{\lambda}{1-\lambda}\mu_0+2$ as the oblique asymptote, is decreasing in the interval $(1-\lambda, \mu_0^*(\lambda))$ and increasing in the interval $(\mu_0^*(\lambda), +\infty)$, where $\mu_0^*(\lambda)$ is defined as (19).
3. The two curves $\mu_1 = m_0(\mu_0)$ and $\mu_1 = m(\mu_0)$ intersect at $(\mu_0, \mu_1) = (\mu_0^*(\lambda), \mu_1^*(\lambda))$, and $m_0(\mu_0) > m(\mu_0)$ when $1-\lambda < \mu_0 < \mu_0^*(\lambda)$; $m_0(\mu_0) < m(\mu_0)$ when $\mu_0 > \mu_0^*(\lambda)$. Furthermore, direct calculations show that $\mu_1^*(\lambda) > \lambda + 2$.

Define R_2 and R_3 such that $B_2 = B^+(R_2)$ and $B_3 = B^+(R_3)$, where B_2, B_3 are defined in Lemmas 2.10 and 2.11. Now we give the proof of Theorems 2.5 and 2.6.

Proof of Theorem 2.5. Note that $\mathrm{Det}(J(w^+, b^+)) > 0$. Then to consider the stability of (w^+, b^+) we just need to consider the sign of the trace of $J(w^+, b^+)$, which has the same sign with $\tilde{f}(B^+)$.

If $(\mu_0, \mu_1) \in \mathrm{I}$, we consider the sign of $\tilde{f}(B^+)$ in three subregions $\mathrm{I}^1, \mathrm{I}^2$ and I^3, where

$$\mathrm{I}^1 = \left\{(\mu_0, \mu_1) : 0 < \mu_0 \le 1-\lambda, \mu_1 > \frac{\lambda\mu_0}{1-\lambda}\right\};$$

$$\mathrm{I}^2 = \left\{(\mu_0, \mu_1) : 1-\lambda < \mu_0 < \frac{(1-\lambda)(\lambda+2)}{\lambda}, \frac{\lambda\mu_0}{1-\lambda} < \mu_1 < \min\{m_0(\mu_0), m(\mu_0)\}\right\};$$

$$\mathrm{I}^3 = \left\{(\mu_0, \mu_1) : \mu_0^* < \mu_0 < \mu_0^{**}, \max\{m_0(\mu_0), \frac{(1-\lambda)(\lambda+2)}{\lambda}\} < \mu_1 < \mu_1^*\right\}.$$

Then $\mathrm{I} = \mathrm{I}^1 \bigcup \mathrm{I}^2 \bigcup \mathrm{I}^3 = \mathrm{I}_1 \bigcup \mathrm{I}_2$, where $\mathrm{I}_1, \mathrm{I}_2$ are defined as in (21). If $(\mu_0, \mu_1) \in \mathrm{I}^1$ then $f(b^+) < 0$ by the expression of $f(b^+)$. If $(\mu_0, \mu_1) \in \mathrm{I}^2$, then $B_* > 1$ by Lemma 2.12 part 1, $\tilde{f}(B_*) < 0$ by Lemma 2.12 part 4, $B_* > B_{**}$ by Lemma 2.12 part 3. Then the conclusion follows from Lemma 2.10 part 1. If $(\mu_0, \mu_1) \in \mathrm{I}^3$, then $B_* > 1$ by Lemma 2.12 part 1, $\tilde{f}(B_*) < 0$ by Lemma 2.12 part 4, $B_* < B_{**}$ by Lemma 2.12 part 3 and $\tilde{f}(B_{**}) < 0$ by Lemma 2.12 part 5. Then the conclusion follows from Lemma 2.10 part 3.

If $(\mu_0, \mu_1) \in \mathrm{II}$, then $\tilde{f}(B_*) > 0$ by Lemma 2.12 part 4 and the conclusion follows from Lemma 2.10 part 4.

If $(\mu_0, \mu_1) \in \mathrm{III}$, then $B_* > 1$ by Lemma 2.12. 1, $B_* < B_{**}$ by Lemma 2.12 part 3, $\tilde{f}(B_*) < 0$ by Lemma 2.12 part 4, $\tilde{f}(B_{**}) > 0$ by Lemma 2.12 part 5. Then the conclusion follows from Lemma 2.10 part 2.

If $(\mu_0, \mu_1) \in \mathrm{IV}$, then $B_* < 1$ by Lemma 2.12 part 1, $\tilde{f}(B_*) < 0$ by Lemma 2.12 part 4, $\tilde{f}(B_{**}) < 0$ by Lemma 2.12 part 5. Then the conclusion follows from Lemma 2.11 parts 1 and 2.

If $(\mu_0, \mu_1) \in \mathrm{V}$, then $B_* < 1$ by Lemma 2.12 part 1, $B_{**} > 1$ by Lemma 2.12 part 2, $\tilde{f}(B_{**}) > 0$ by Lemma 2.12 part 5. Then the conclusion follows from Lemma 2.11 part 3. □

Proof of Theorem 2.6. When $\lambda \ge 1$, we consider $B \in [1, \infty)$. Note that $\mu_1^* > \lambda + 2$ and $\tilde{f}(1) < 0$. If $(\mu_0, \mu_1) \in \mathrm{VI}$, then $\tilde{f}(B_{**}) < 0$ by Lemma 2.12. 5. Similar to Lemma 2.11. 1 and 2, we have $\tilde{f}(B) < 0$ which implies the stability of (w^+, b^+) if $(\mu_0, \mu_1) \in \mathrm{VI}$.

If $(\mu_0, \mu_1) \in \mathrm{VII}$, then $\tilde{f}(B_{**}) > 0$ by Lemma 2.12. 5. Similar to Lemma 2.11. 3, there exist $1 < B_2 < B_{**} < B_3$ such that $\tilde{f}(B) < 0$ for $B \in [1, B_2) \bigcup (B_3, \infty)$

and $\tilde{f}(B) > 0$ for $B \in (B_2, B_3)$, which implies that there exist R_2, R_3 with $R_0 < R_2 < R_3$ such that (w^+, b^+) is unstable when $R_2 < R < R_3$, and it is locally asymptotically stable when $R_0 < R < R_2$ or $R > R_3$. □

3. **Hopf bifurcations and homoclinic bifurcations.** From Theorem 2.5 and Theorem 2.6, there exist values of R, which denoted by $R_i, i = 2, 3$ such that the corresponding characteristic matrix has a pair of complex roots, denoted by $\sigma(R)$,

$$\sigma(R) = \alpha(R) \pm i\omega(R),$$

where

$$\alpha(R) = \frac{1}{2}\left[\frac{b^+\mu_1}{(b^+ + 1)^2} - (\lambda b^+ + 1)\right],$$

$$\omega(R) = \sqrt{\frac{\lambda R b^+}{\lambda b^+ + 1} - \frac{1}{4}\left(\frac{b^+\mu_1}{(b^+ + 1)^2} + \lambda b^+ + 1\right)^2}.$$

From last section, we have

$$\alpha(R_i) = \left(\frac{1}{2(B^+)^2}\tilde{f}(B^+)\right)\Big|_{R=R_i} = 0, \quad i = 2, 3,$$

$$\alpha'(R_i) = \left(\frac{1}{2(B^+)^2}\tilde{f}(B^+)\right)'\Big|_{R=R_i} = \left(\frac{1}{2(B^+)^2}\tilde{f}'(B^+)\right)\Big|_{R=R_i} \neq 0, \quad i = 2, 3,$$

where $\tilde{f}(B)$ is defined as (37). Here, we use the fact that $\tilde{f}'(B_2) > 0$ and $\tilde{f}'(B_3) < 0$ which result in $\alpha'(R_2) > 0$ and $\alpha'(R_3) < 0$. Then we conclude that a Hopf bifurcation occurs at $R = R_i, i = 2, 3$.

Theorem 3.1. *Assume that the parameters R, λ, μ_0, μ_1 are all positive and $R = R_i, i = 2, 3$ are as defined in Theorems 2.5 and 2.6. Then system (3) undergo a Hopf bifurcation at R_2 and R_3 if exists.*

We note that there are well-established methods (see [8, 24]) to determine the direction of the Hopf bifurcations at $R = R_2$ and $R = R_3$. Here we omit the detailed procedure as the computation is tedious and inconclusive. In the following we show by cases and examples that both supercritical and subcritical Hopf bifurcations can occur for different parameter ranges.

First when (μ_0, μ_1) is in the parameter regions III, V, or VII, there are two Hopf bifurcation points $R = R_2$ and $R = R_3$. In this case, a bounded branch of limit cycles emerges from the equilibrium (w^+, b^+) at $R = R_2$ and returns to the same equilibrium at $R = R_3$, so the branch is a loop or a "bubble". In Figure 5, the bifurcation diagrams and phase portraits of limit cycles for three sets of parameters in III, V, and VII respectively are shown. In each case, the bifurcation diagram (produced with `MatCont`) in the left panel shows two Hopf bifurcation points (labelled by "H"), and the numerically calculated first Lyapunov coefficients at both bifurcation points are negative in all three cases so the bifurcating periodic orbits are stable ones. Note that in Figure 5 (a)-(b), the dynamics is bistable with a stable limit cycle and a stable equilibrium $(R, 0)$ when $R_2 < R < R_3$, while in (c)-(d) and (e)-(f), the limit cycle is globally asymptotically stable when $R_2 < R < R_3$. In all cases shown in Figure 5, the limit cycle appears to be unique, though we do

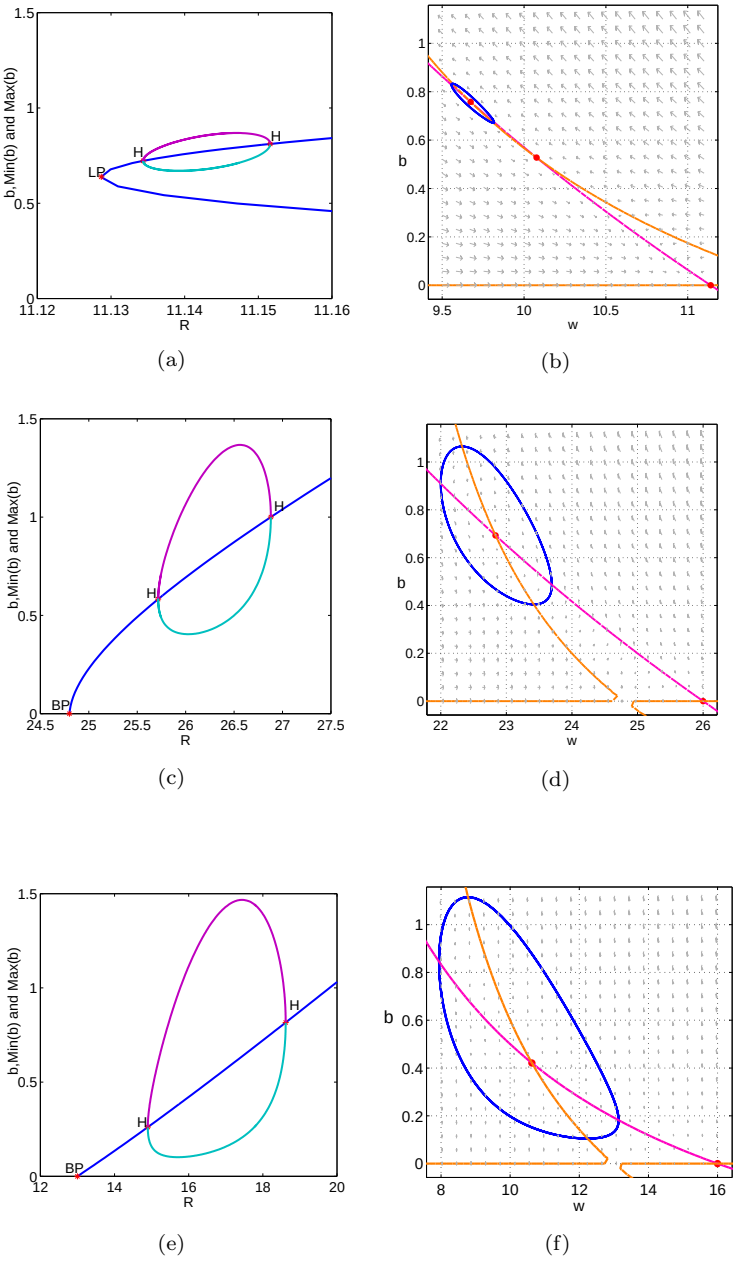

FIGURE 5. Bifurcation diagrams (bubble branch of cycles) and phase portraits of limit cycles when there are two Hopf bifurcation points $R = R_2$ and $R = R_3$. In (a), (c) and (e), the blue curve, the cyan curve and the purple curve represent the biomass b, the minimum value and the maximum value of b of the limit cycles versus the rain-fall rate R, respectively; corresponding phase portraits are shown in (b), (d) and (f). In (a) and (b) $\lambda = 0.2$, $(\mu_0, \mu_1) = (7, 4.7) \in$ III, and $R = 11.14$ in (b); in (c) and (d) $\lambda = 0.2$, $(\mu_0, \mu_1) = (20, 4.8) \in$ V, and $R = 26$ in (d); and in (e) and (f) $\lambda = 1.2$, $(\mu_0, \mu_1) = (5, 8) \in$ VII, and $R = 16$ in (f).

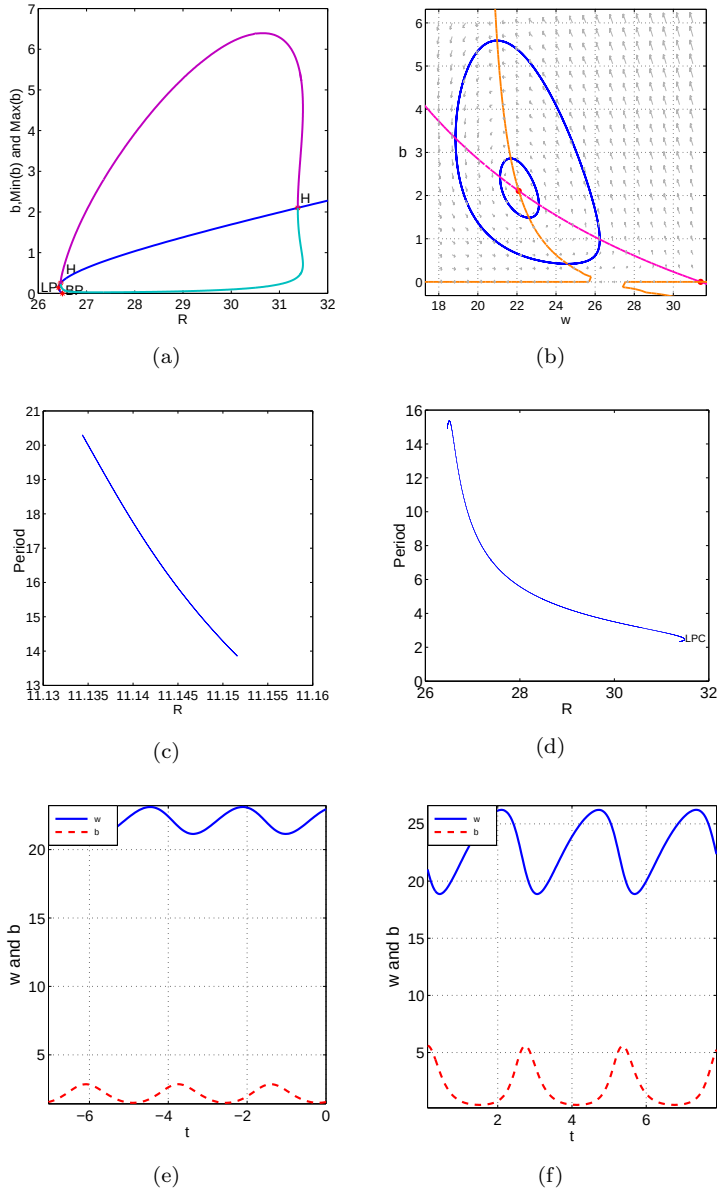

FIGURE 6. Hopf bifurcation and multiple limit cycles when $\lambda = 0.2$ and $(\mu_0, \mu_1) \in$ III. (a): The bifurcation diagram when $(\mu_0, \mu_1) = (20, 6.5) \in$ III. The blue curve, the cyan curve and the purple curve represent the biomass b, the minimum value and the maximum value of b of the limit cycles vs. the rainfall rate R, respectively. (b): Two limit cycles when $(\mu_0, \mu_1) = (20, 6.5) \in$ III and $R = 31.4$. (c): Period of limit cycles versus R when $(\mu_0, \mu_1) = (7, 4.7) \in$ III, and the period is monotonically decreasing in R. (d): Period of limit cycles versus R when $(\mu_0, \mu_1) = (20, 6.5) \in$ III, and the period is not monotone in R and is not single-valued (indicating multiple limit cycles). (e): Time series of the small amplitude periodic orbit when $(\mu_0, \mu_1) = (20, 6.5) \in$ III and $R = 31.4$. (f): Time series of the large amplitude periodic orbit when $(\mu_0, \mu_1) = (20, 6.5) \in$ III and $R = 31.4$.

not have an analytic proof of that. For the parameter values in Figure 5 (a)-(b), the period of the (unique) limit cycle is decreasing in R as shown in 6 (c).

In Figure 6 (a)-(b), the bifurcation diagram and phase portrait of limit cycles for a different value $(\mu_0, \mu_1) \in$ III is shown. Here the Hopf bifurcation at $R = R_2$ is supercritical but the one at $R = R_3$ is subcritical. The branch of limit cycles is still a closed loop but we call it a "heart" to indicate the existence of multiple periodic orbits for some values of R. Indeed here a saddle-node bifurcation for the periodic orbits occurs at some $R = R_4 > R_3$, and there exist two periodic orbits for $R_3 < R < R_4$ (see Figure 6 (b) for phase portrait and Figure 6 (e)-(f) for the time series of the two periodic orbits). The dependence of period of periodic orbits on R is shown in 6 (d): for R close to R_2, the period appears to be not monotone, and for R close to R_3, the period is multi-valued as there are multiple periodic orbits.

Secondly, if (μ_0, μ_1) is in the parameter region II, then there is only one Hopf bifurcation point $R = R_3$. Here the branch of limit cycles is not a closed loop as in the "bubble" or the "heart" case above, but is an "open-ended" one. However the results in Proposition 2.8 imply that there is no periodic orbits for large R or small R, hence the branch of periodic orbits is bounded in R direction. On the other hand, Lemma 2.1 implies that all periodic orbits are bounded on the phase plane for bounded R values. Then from the global Hopf bifurcation theorem [1, 5], the period of the periodic orbits on the bifurcating branch must be unbounded. We call such a bifurcation diagram a "lotus" with the Hopf bifurcation point as the base and the homoclinic bifurcation point the top of the lotus. In Figure 7 (a)-(b) and (c)-(d), the bifurcation diagrams and phase portraits of limit cycles for two different $(\mu_0, \mu_1) \in$ II are shown. For $(\mu_0, \mu_1) \in$ II, there is always a saddle-node bifurcation point at $R = R_1$, which is labeled by "LP" in Figure 7 (a) and (c). The Hopf bifurcation at $R = R_3$ can be supercritical as in (a), or subcritical as in (c). In the former case, the bifurcating periodic orbits are stable while in the latter case they are unstable. In Figure 7 (e) and (f), one can observe that the period of cycles is increasing in R for the bifurcation diagram corresponding to (a), and the period is decreasing in R for the one corresponding to (c). In both cases, the period approach to ∞ when R tends to some $R = R_{HL}$, which is a homoclinic bifurcation point where the limit cycles converge to a homoclinic orbit based on the saddle equilibrium (w^-, b^-). This can be observed in Figure 7 (a) and (c) as the limit of minimum of the cycles is the lower positive equilibrium. Note that the sequence of Hopf bifurcation and homoclinic bifurcation is also the signature of the codim-2 Bogdanov-Takens bifurcation, which will be discussed later.

Figure 8 shows the evolution of phase portraits of system (3) with $\lambda = 0.2$ and $(\mu_0, \mu_1) = (5, 5.2) \in$ II (which is the one in Figure 7 (a)) when R increases. One can easily calculate that the bifurcation values $R_0 = 10.2$ (backward transcritical bifurcation point), $R_1 = 9.119216$ (saddle-node bifurcation point), and $R_3 = 9.161059$ (Hopf bifurcation point). Here the Hopf bifurcation is subcritical so the bifurcating periodic orbits are unstable. Moreover the homoclinic bifurcation point is $R_{HL} = 9.1830408$. Apparently when $0 < R < R_1$, the bare-soil equilibrium $(R, 0)$ is the attractor; when $R_1 < R < R_3$, both positive equilibria (w^+, b^+) (unstable node) and (w^-, b^-) (saddle) are unstable, and all positive orbits except the positive equilibria and the stable manifold (the green orbits) of (w^-, b^-) tend to the trivial bare soil equilibrium $(w_0, b_0) = (R, 0)$ (see Figure 8 (a)); when R increases to $R_3 < R < R_{HL}$, the equilibrium (w^+, b^+) becomes stable and an unstable limit cycle emerges from the subcritical Hopf bifurcation (see Figure 8 (b)). In this case,

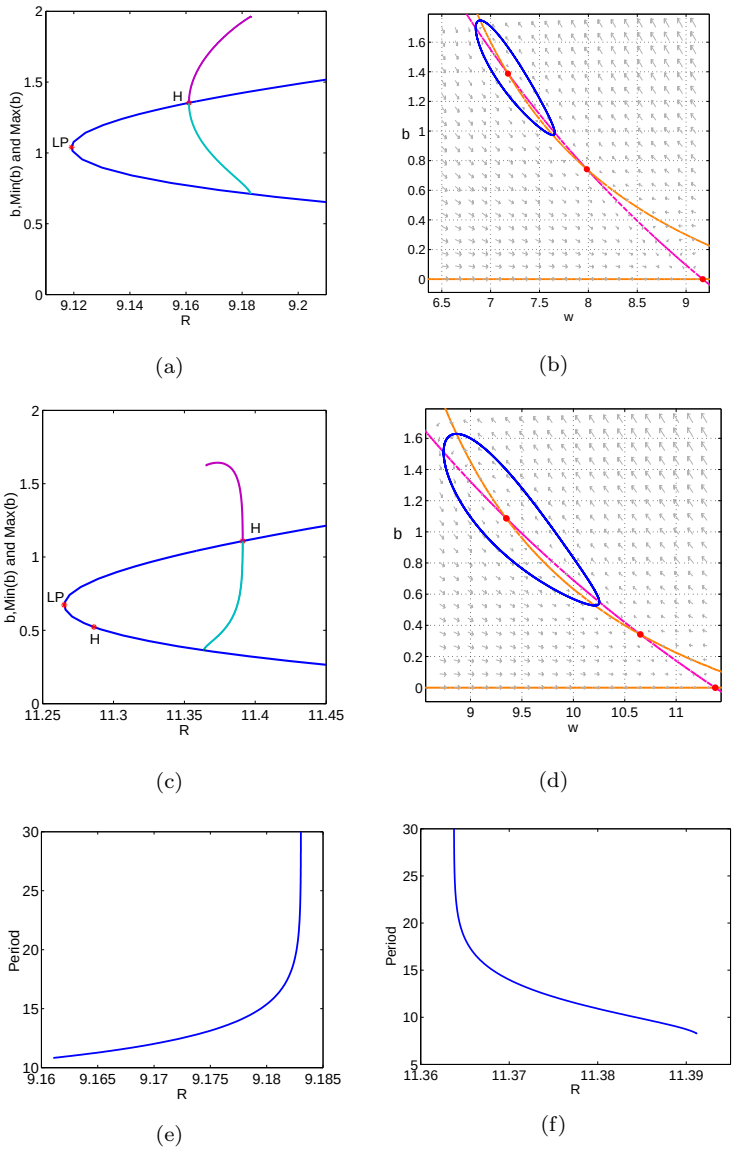

FIGURE 7. Homoclinic bifurcation, saddle-node bifurcation, Hopf bifurcation and the existence of one limit cycle when $\lambda = 0.2$ and $(\mu_0, \mu_1) \in$ II. In (a), (c), the blue curve, the cyan curve and the purple curve represent the biomass b, the minimum value and the maximum value of b of the limit cycles vs. the rain-fall rate R, respectively. (a): Bifurcation diagram when $(\mu_0, \mu_1) = (5, 5.2) \in$ II. (b): Phase portrait with periodic orbit when $(\mu_0, \mu_1) = (5, 5.2)$ and $R = 9.17$. (c): Bifurcation diagram when $(\mu_0, \mu_1) = (7, 4.9) \in$ II. (d): Phase portrait with periodic orbit when $(\mu_0, \mu_1) = (7, 4.9)$ and $R = 11.38$. (e): Period of the stable periodic orbits when $(\mu_0, \mu_1) = (5, 5.2)$. (f): Period of the unstable limit cycles when $(\mu_0, \mu_1) = (7, 4.9)$.

the unstable cycle serves as the separatrix between the basins of attraction of the equilibria (w^+, b^+) and $(R, 0)$. At $R = R_{HL}$, a homoclinic orbit exists and it is the separatrix between the basins of attraction of the equilibria (w^+, b^+) and $(R, 0)$ (see Figure 8 (c)). When R increases to $R_{HL} < R < R_0$, the basins of attraction for the two locally stable equilibria are separated by the stable manifold of the saddle equilibrium (w^-, b^-) (see Figure 8 (d)). In each of Figure 8 (b), (c) and (d), system (3) has a bistability of the bare-soil equilibrium $(R, 0)$ and the positive equilibrium (w^+, b^+), but the separatrix is different. When $R > R_0$, the system is monostable as all solutions tend to the positive equilibrium (w^+, b^+).

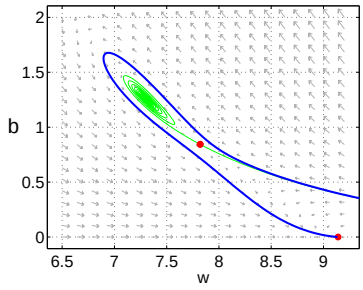

(a) $R_1 < R < R_3$.

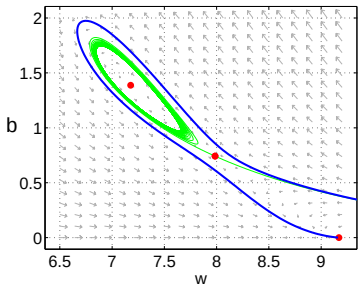

(b) $R_3 < R < R_{HL}$.

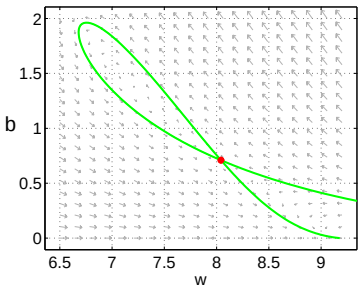

(c) $R = R_{HL}$.

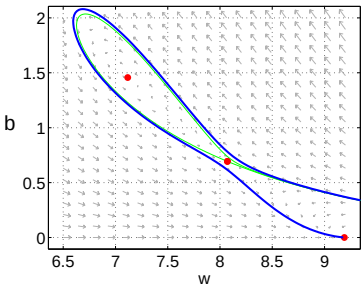

(d) $R_{HL} < R < R_0$.

FIGURE 8. Evolution of phase portraits of (3) for $\lambda = 0.2$, $(\mu_0, \mu_1) = (5, 5.2) \in$ II and $R > R_1$. (a) $R = 9.14$; (b) $R = 9.17$; (c) $R = 9.1830408$; (d) $R = 9.19$.

On the other hand, Figure 9 shows the evolution of phase portraits of system (3) with $\lambda = 0.2$ and $(\mu_0, \mu_1) = (7, 4.9) \in$ II (which is the one in Figure 7 (c)) when R increases. Now the bifurcation values are $R_0 = 11.9$, $R_1 = 11.265296$, and $R_3 = 11.391151$ and the Hopf bifurcation at $R = R_3$ is supercritical. Furthermore the homoclinic bifurcation point is $R_{HL} = 11.363757$. When $R > R_3$, the equilibrium (w^+, b^+) is stable in Figure 9 (d). Then system (3) admits the bistability of the bare-soil equilibrium and a positive equilibrium when $R_3 < R < R_0$ and the region of attraction for these equilibria are separated by the separatrix (the green orbits) of saddle (w^-, b^-). As R decreases to $R_{HL} < R < R_3$, the equilibrium (w^+, b^+) becomes unstable and a stable limit cycle emerges from a supercritical Hopf bifurcation in Figure 9 (c). In this case, system (3) admits the bistability of the bare-soil

equilibrium and a stable limit cycle with the stable manifolds (the green orbits) of the saddle (w^-, b^-) as the separatrix of attraction. When R decreases to R_{HL}, the period of the limit cycle tends to infinity and a homoclinic orbit emerges in Figure 9 (b). As R decreases to $R_1 < R < R_{HL}$, the homoclinic orbit is broken and the equilibrium (w^+, b^+) is still unstable. All of the positive orbits except for positive equilibria $(w^\pm, b^\pm)$ and stable manifold (the green orbits) of (w^-, b^-) tend to the trivial bare-soil equilibrium $(w_0, b_0) = (R, 0)$ in Figure 9 (a).

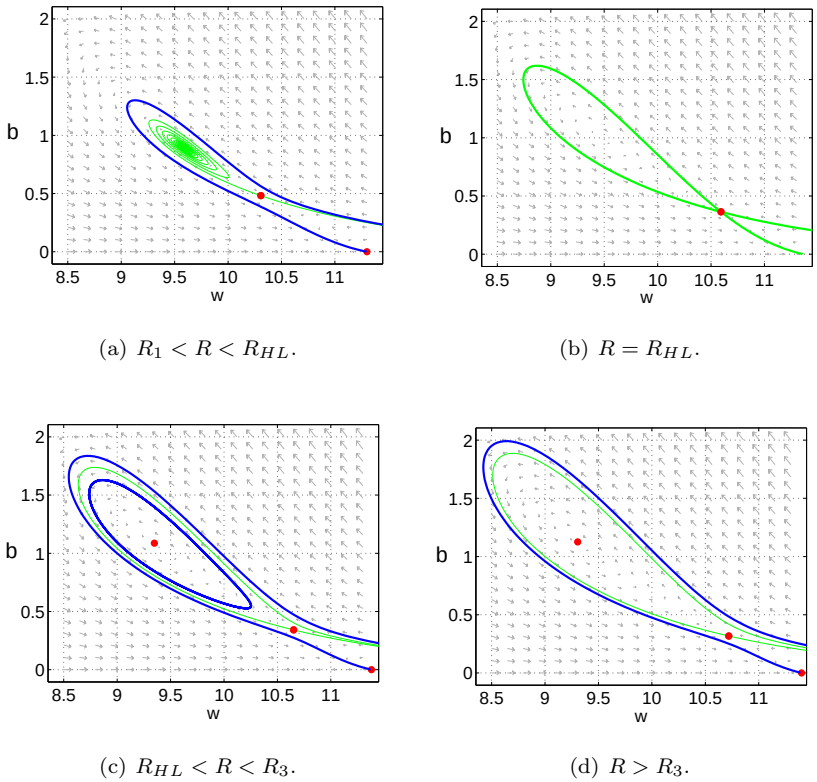

(a) $R_1 < R < R_{HL}$. (b) $R = R_{HL}$.

(c) $R_{HL} < R < R_3$. (d) $R > R_3$.

FIGURE 9. Evolution of phase portraits of (3) for $\lambda = 0.2$ and $(\mu_0, \mu_1) = (7, 4.9) \in$ II and $R > R_1$. (a) $R = 11.3$; (b) $R = 11.363757$; (c) $R = 11.38$; (d) $R = 11.4$.

Finally we mention that homoclinic bifurcation and multiple periodic orbits can occur for the same (μ_0, μ_1) value. In Figure 10, the bifurcation diagram and phase portraits of limit cycles are shown for $\lambda = 0.2$ and $(\mu_0, \mu_1) = (7, 5) \in$ II. Here a subcritical Hopf bifurcation occurs at $R = R_3$. In some range of R only one stable limit cycle exists (Figure 10 (b)), and the multi-valued period of the limit cycles in Figure 10 (c) implies that two periodic orbits can coexist (Figure 10 (d)). The period of the limit cycles tend to infinity at a critical value $R_{HL} = 11.47377$ which is the homoclinic bifurcation point. Time series of the two limit cycles for the same parameter values are shown in Figure 10 (e) and (f). We call this bifurcation diagram a "pepper" as it resembles the shape of bell pepper.

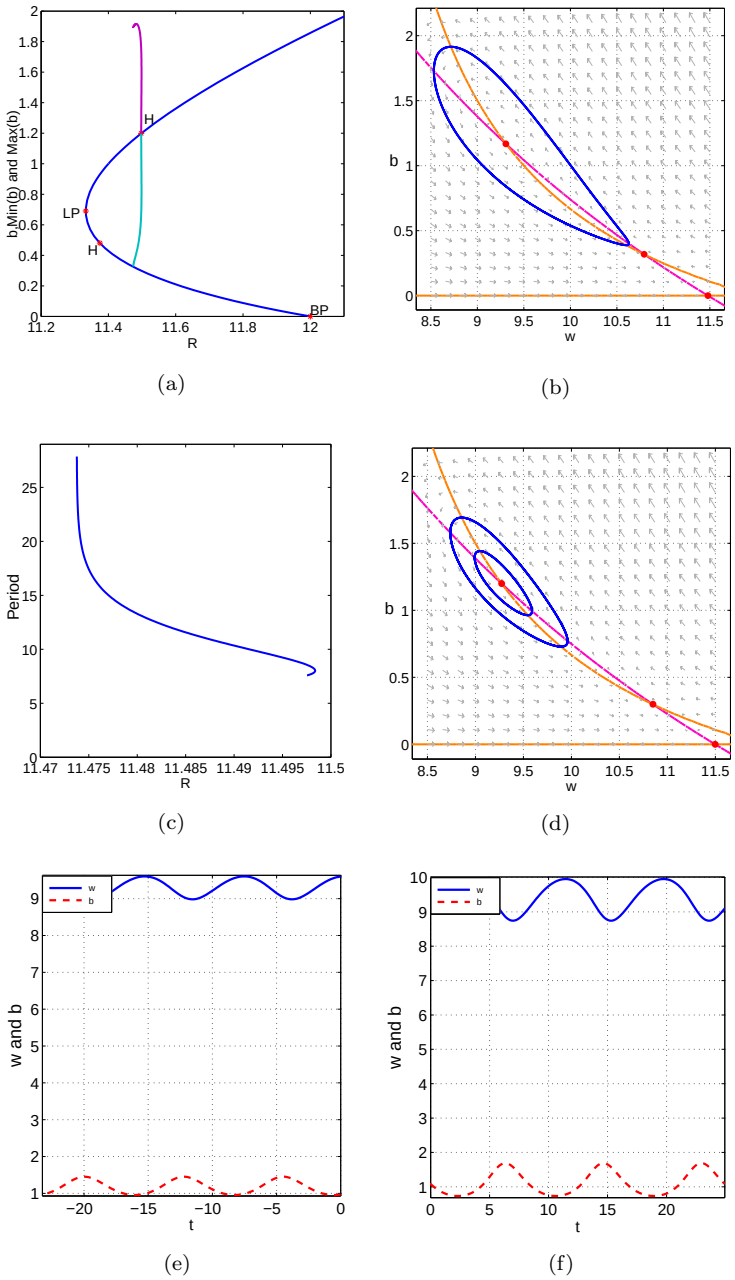

FIGURE 10. Homoclinic bifurcation, saddle-node bifurcation, Hopf bifurcation and multiple limit cycles for $\lambda = 0.2$ and $(\mu_0, \mu_1) = (7, 5) \in$ II. (a): The bifurcation diagram. The blue curve, the cyan curve and the purple curve represent the biomass b bifurcation diagram, the minimum value and the maximum value of b of the limit cycles vs. the rain-fall rate R, respectively. (b): Phase portrait with one stable limit cycle when $R = 11.48$. (c): Period of limit cycles versus R. (d): Phase portrait with two limit cycles when $R = 11.498$. (e): Time series of the small amplitude periodic orbit when $R = 11.498$. (f): Time series of the large amplitude periodic orbit when $R = 11.498$.

Figure 11 shows the evolution of phase portraits when $\lambda = 0.2$ and $(\mu_0, \mu_1) = (7, 5) \in$ II (the one in Figure 10). The bifurcation points are $R_0 = 12$, $R_1 = 11.332864$, and $R_3 = 11.497537$ and the Hopf bifurcation is subcritical. Two additional bifurcation points which cannot be analytically solved are the limit cycle saddle-node bifurcation point $R_{LPC} = 11.49838$ and the homoclinic bifurcation point $R_{HL} = 11.47377$. Some parts of evolution are same as the ones in Figure 9, but in Figure 11 (d) there are indeed three locally stable states: the positive equilibrium (w^+, b^+), the large amplitude limit cycle, and the bare-soil equilibrium $(R, 0)$. This is the only "tristable" dynamics for (3), while most other cases for (3) are bistable or monostable.

4. **Bogdanov-Takens bifurcation.** So far our bifurcation analysis is through a single bifurcation parameter R with other parameters (λ, μ_0, μ_1) in certain ranges. By using two-parameter unfolding, we can show that a Bogdanov-Takens bifurcation occurs in the system (3). To that end, we fix $\lambda \in (0, 1)$ and $\mu_0 > 0$, and choose μ_1 and R in the following way:

(C_1) $\mu_1 = m(\lambda, \mu_0)$ which is defined in (18);
(C_2) $R = R_1(\lambda, \mu_0, \mu_1(\lambda, \mu_0))$ which is defined in (8).

Then system (3) admits an unique positive equilibrium (w^*, b^*) (at the saddle-node bifurcation point) defined by

$$w^* = \frac{R_1}{\lambda b^* + 1}, \qquad b^* = \frac{\sqrt{\lambda(1-\lambda)\mu_0\mu_1} - \lambda\mu_0}{\lambda\mu_0}, \tag{40}$$

and

$$\mathrm{Det}(J(w^*, b^*)) = (B_* - 1)\tilde{R}'(B_*) = 0, \quad \mathrm{Trace}(J(w^*, b^*)) = \frac{1}{B_*^2}\tilde{f}(B_*) = 0, \tag{41}$$

where $\tilde{f}(B)$ is defined as (37). Therefore, if (C_1) and (C_2) are satisfied then the Jacobian matrix at (w^*, b^*) has a zero eigenvalue with multiplicity 2. This suggests that (3) may admit a Bogdanov-Takens bifurcation. In the following, by similar procedures to those in [18, 35, 36], we confirm that (w^*, b^*) is a cusp singularity of codimension 2.

Theorem 4.1. *Assume that the parameters R, μ_0, μ_1 are all positive, $0 < \lambda < 1$ and μ_0^* is defined as (19). Suppose that (C_1) and (C_2) are satisfied. If $\mu_0 \neq \mu_0^*$, then the equilibrium (w^*, b^*) of (3) is a cusp of codimension 2, i.e. it is a Bogdanov-Takens singularity.*

Proof. By the transformation of $u = w - w^*, v = b - b^*$, and still denoted u, v by w, b, system (3) becomes

$$\begin{cases} \dfrac{dw}{dt} = a_{11}w + a_{12}b - \lambda wb, \\ \dfrac{db}{dt} = b^*w - a_{11}b + wb + a_{20}b^2 + Q_1(w, b), \end{cases} \tag{42}$$

where $Q_1(w, b)$ are smooth functions in (w, b) at least of order three, and

$$a_{11} = -(\lambda b^* + 1), \qquad a_{12} = -\frac{(\lambda b^* + 1)^2}{b^*}, \qquad a_{20} = \frac{\mu_1}{(b^* + 1)^3}.$$

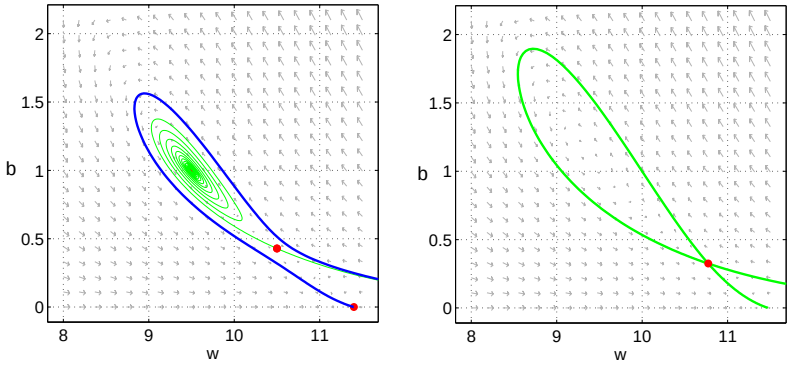

(a) $R_1 < R < R_{HL}$. (b) $R = R_{HL}$.

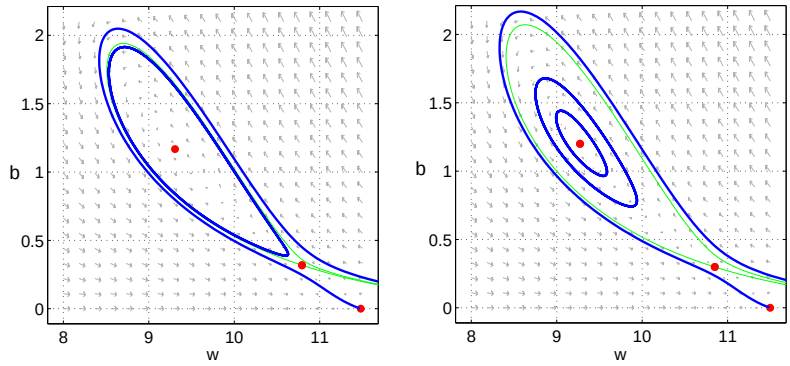

(c) $R_{HL} < R < R_3$. (d) $R_3 < R < R_{LPC}$.

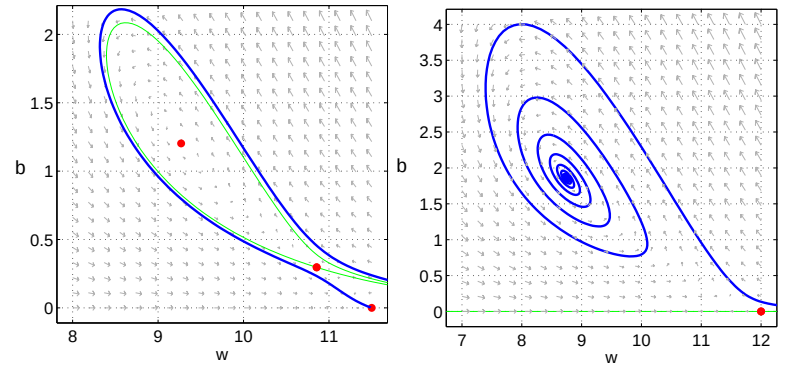

(e) $R_{LPC} < R < R_0$. (f) $R > R_0$.

FIGURE 11. Evolution of phase portraits of (3) for $\lambda = 0.2$, $(\mu_0, \mu_1) = (7, 5) \in$ II and $R > R_1$. (a) $R = 11.4$; (b) $R = 11.47377$; (c) $R = 11.48$; (d) $R = 11.498$; (e) $R = 11.5$; (f) $R = 12$.

Set $u = w$, $v = a_{11}w + a_{12}b$ and rename u, v as w, b respectively. Then (42) is transformed into

$$\begin{cases} \dfrac{dw}{dt} = b + b_1 w^2 + b_2 wb, \\ \dfrac{db}{dt} = c_1 w^2 + c_2 wb + c_3 b^2 + Q_2(w, b), \end{cases} \tag{43}$$

where $Q_2(w, b)$ are smooth functions in (w, b) at least of order three, and

$$b_1 = \frac{\lambda a_{11}}{a_{12}}, \qquad b_2 = -\frac{\lambda}{a_{12}},$$
$$c_1 = \frac{a_{11}(\lambda a_{11} - a_{12} + a_{20}a_{11})}{a_{12}}, \quad c_2 = \frac{a_{12} - \lambda a_{11} - 2a_{20}a_{11}}{a_{12}}, \quad c_3 = \frac{a_{20}}{a_{12}}.$$

Let $u = w$, $v = b - c_3 wb$ and rewrite u, v as w, b respectively. Then system (43) becomes

$$\begin{cases} \dfrac{dw}{dt} = b + b_1 w^2 + (b_2 + c_3) wb + P_3(w, b), \\ \dfrac{db}{dt} = c_1 w^2 + c_2 wb + Q_3(w, b), \end{cases} \tag{44}$$

where $P_3(w, b), Q_3(w, b)$ are smooth functions in (w, b) at least of order three. Finally by the transformation of $u = w - \dfrac{b_2 + c_3}{2} w^2, v = b + b_1 w^2$ and rewrite u, v as w, b respectively, system (44) becomes

$$\begin{cases} \dfrac{dw}{dt} = b + P_4(w, b), \\ \dfrac{db}{dt} = c_1 w^2 + (c_2 + 2b_1) wb + Q_4(w, b), \end{cases} \tag{45}$$

where $P_4(w, b), Q_4(w, b)$ are smooth functions in (w, b) at least of order three.

Note that

$$c_1 = \frac{\mu_1 b^* (1 - \lambda)^2 (\mu_0 - (1 - \lambda))}{(b^* + 1)^2 \mu_0 (\mu_0 \lambda + (1 - \lambda)^2)} > 0,$$

and

$$c_2 + 2b_1 = \frac{1}{\mu_0(\mu_0\lambda + (1 - \lambda)^2)} \left[-\lambda \mu_0^2 + (1 - \lambda)(1 + 2\lambda)\mu_0 + (1 - \lambda)^3 \right] \neq 0,$$

if $\mu_0 \neq \mu_0^*$. Thus, it follows from [16, Lemma 8.6] that the equilibrium (w^*, b^*) of (2.1) is a cusp of codimension 2, *i.e.* it is a Bogdanov-Takens singularity if $\mu_0 \neq \mu_0^*$. □

Theorem 4.1 implies that system (3) may admit a Bogdanov-Takens bifurcation. From [16, Theorem 8.4] and symbolic calculation in `Maple`, we can find the versal unfolding and approximating bifurcation curves depending on the original parameters for (2.1) near the Bogdanov-Takens bifurcation point (see Appendix for details).

Figure 12 illustrates the Bogdanov-Takens bifurcation in the $R - \mu_1$ plane for several (λ, μ_0) values. In each panel of Figure 12, the cyan curve Γ_1 represents the Hopf bifurcation curve, the blue curve Γ_2 represents the saddle-node bifurcation curve (which only exists when $0 < \lambda < 1$) and the black line Γ_3 is the transcritical bifurcation curve $R = R_0 = \mu_1 + \mu_0$. When $0 < \lambda < 1$, the saddle-node curve Γ_1 and the Hopf curve Γ_2 divide the $R - \mu_1$ plane into three parts, marked by "nonexistence" (no positive equilibrium), "stable" ((w^+, b^+) is stable) and "unstable" ((w^+, b^+) is unstable), respectively (see Figure 12 (a), (b) and (c)). The line Γ_3 separates the

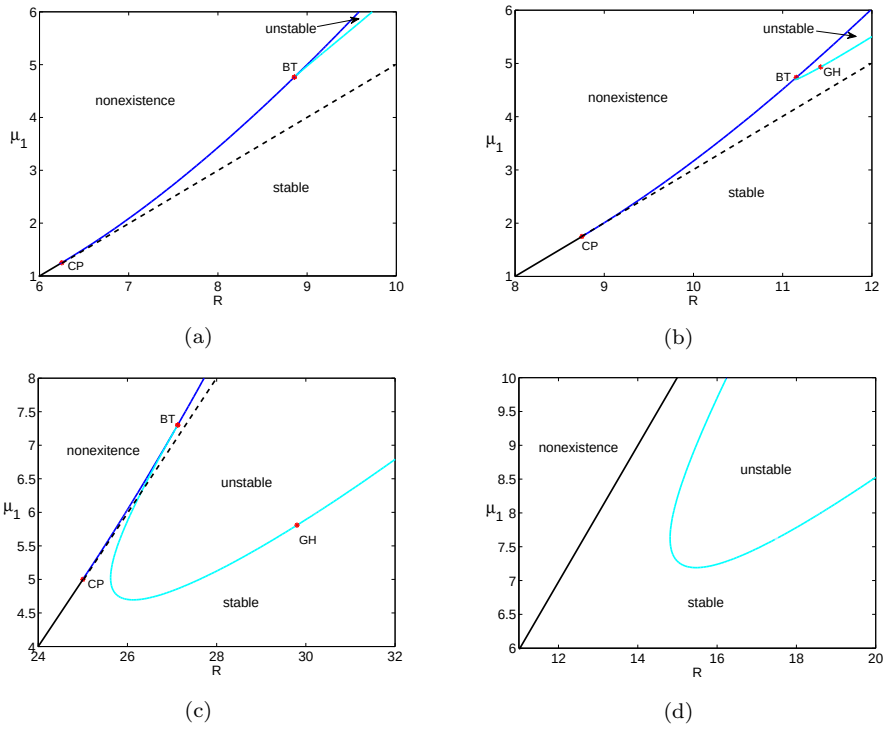

FIGURE 12. The cyan curve represents the Hopf bifurcation curve, the blue curve represents the saddle-node bifurcation curve and the black line is $\mu_1 = R - \mu_0$. The "BT" mark indicates a Bogdanov-Takens bifurcation point; the "CP" mark indicates a cusp bifurcation point; and the "GH" mark indicates a generalized Hopf point where the first Lyapunov coefficient vanishes while the second Lyapunov coefficient does not vanish, which indicates that it is nondegenerate, i.e. Hopf bifurcation changes from subcritical to supercritical. (a): $\lambda = 0.2, \mu_0 = 5$. (b): $\lambda = 0.2, \mu_0 = 7$. (c): $\lambda = 0.2, \mu_0 = 20$. (d): $\lambda = 1.2, \mu_0 = 5$.

parameter regions with 1 or 2 positive equilibria. The intersection point of the saddle-node curve Γ_1 and the Hopf curve Γ_2 is the Bogdanov-Takens bifurcation point marked by "BT", and the intersection of Γ_2 and Γ_3 is the cusp bifurcation point marked by "CP" (again by using package `MatCont`). Another degenerate bifurcation point marked by "GH" is the generalized Hopf bifurcation point where the first Lyapunov coefficient vanishes while the second Lyapunov coefficient does not vanish, and that is where the Hopf bifurcation changes from subcritical to supercritical. In Figure 12 (a), the Hopf bifurcation curve is a monotone curve, which implies that there is only one Hopf bifurcation point $R = R_3$ when using R as bifurcation parameter. On the other hand, in Figure 12 (c) the Hopf bifurcation curve is not monotone which means that there may exist two Hopf bifurcation points $R = R_2$ and $R = R_3$. In Figure 12 (c), the Hopf bifurcation curve Γ_1 also intersects with the transcritical bifurcation curve Γ_3, which means that the Hopf bifurcation points R_2 and R_3 may be larger than R_0.

Figure 12 (d) shows the case of $\lambda \geq 1$. Here the $R - \mu_1$ plane is divided by the Hopf bifurcation curve Γ_1 and the transcritical bifurcation curve Γ_3. There is no

Bogdanov-Takens bifurcation point here as there is no saddle-node bifurcation point, and we suspect all Hopf bifurcations are supercritical so there is no generalized Hopf bifurcation point. Note that Figure 12 does not exhaust all possible situations, but in other cases (as shown in Theorems 2.5 and 2.6), there is no Hopf bifurcation curve then the dynamics is simpler.

5. **Conclusions.** We propose an ordinary differential equation model (3) for the interaction between a plant (shrubs or trees) and a resource (water). The biomass death rate is assumed to be decreasing respect to the biomass in order to capture the infiltration feedback [6, 7]. We find rich bifurcation structure in (3) including (forward/backward) transcritical bifurcations, saddle-node bifurcations, (subcritical/supercritical) Hopf bifurcations, homoclinic bifurcation, and Bogdanov-Takens bifurcations. The type of bifurcations are listed in Table 1 according to the values of (μ_0, μ_1) in different regions.

TABLE 1. Results of bifurcation points.

λ	(μ_0, μ_1)	Transcritical at $R = R_0$	Saddle-node bifurcation	Hopf bifurcation points	Homoclinic bifurcation	B-T bifurcation
$0 < \lambda < 1$	I	backward	R_1	none	none	R_1
$0 < \lambda < 1$	II	backward	R_1	R_3	exist	R_1
$0 < \lambda < 1$	III	backward	R_1	R_2, R_3	none	R_1
$0 < \lambda < 1$	IV	forward	none	none	none	none
$0 < \lambda < 1$	V	forward	none	R_2, R_3	none	none
$\lambda \geq 1$	VI	forward	none	none	none	none
$\lambda \geq 1$	VII	forward	none	R_2, R_3	none	none

From analysis and simulations, system (3) admits monostable, bistable or tristable dynamics. There exist bistable regions in which the bare-soil equilibrium coexists with a positive equilibrium, *i.e.* the extinction of the biomass coexists with the "steady state persistence" of the biomass, or the bare-soil equilibrium coexists with a stable limit cycle, *i.e.* the extinction of the biomass coexists with the "oscillatory persistence" of the biomass, or the positive equilibrium coexists with a stable limit cycle, and tristable regions in which two equilibria coexist with one limit cycle. In the bistable and tristable parameter regions, the asymptotic biomass is determined by the initial water and biomass density.

A hysteresis loop exists in the model (3) if the rain-fall rate varies. When the rain-fall rate is high, the system stays at a high vegetation equilibrium; when the rain-fall rate drops, the vegetation equilibrium decreases and it may switch to a oscillatory state; when the rain-fall rate further decreases, the oscillatory state may shrink back to an equilibrium (Figure 3 (d)-(e)), or may suddenly go to global extinction (Figure 3 (f)-(h)). In the former case, the high vegetation state will also disappear in the saddle-node bifurcation. So either case lead to a catastrophic shift. But in both scenarios, time-periodic pattern occurs, which may be an early indicator of the catastrophic shift. Previous work on catastrophic shifts focus on mostly equilibrium behavior changes in the models (without spatial effect) [14, 28, 31], and our work indicates that time-periodic pattern is also an important state for such systems. System (3) provides a fundamental theoretical foundation for alternative stable states and oscillations in species-resource systems, and it will also serve as a basic kinetic model for spatiotemporal pattern formation with effect of diffusion, cross-diffusion and nonlocal dispersal.

As mentioned earlier, our model (3) can also be considered as an epidemic model. Indeed one can consider an SIR epidemic model with birth/death and treatment:

$$\begin{cases} \dfrac{dS}{dt} = a - \alpha SI - aS, \\ \dfrac{dI}{dt} = \alpha SI - \beta I - aI - \dfrac{bI}{1+cI}, \\ \dfrac{dR}{dt} = \beta I - aR + \dfrac{bI}{1+cI}, \end{cases} \tag{46}$$

where $\alpha, \beta, a, b, c > 0$. Then methods used in this paper can also be applied to (46). Similar SIR epidemic models with treatment have been considered in [32, 34, 38, 39]. Backward bifurcation has been observed in all these models, and some also studied Hopf bifurcation and existence/nonexistence of limit cycles. But none of these work considered limit cycle bubble, homoclinic bifurcation, and Bogdanov-Takens bifurcation. By using our methods here, one can also obtain a detailed partition of the parameter space and classify the dynamics of (46) into various bifurcation diagrams including "bubble", "heart", "lotus" and "pepper".

Appendix A. **Approximating bifurcation curves.** We choose R and μ_1 as bifurcation parameters. Suppose R, μ_1, μ_0, λ satisfy (C_1) and (C_2). Let

$$\begin{aligned} &R = R_1 + \lambda_1, \qquad \mu_1 = m(\mu_0) + \lambda_2, \\ &w^* = \frac{R_1}{\lambda b^* + 1}, \qquad b^* = \frac{\sqrt{\lambda(1-\lambda)\mu_0 m_1} - \lambda\mu_0}{\lambda\mu_0}. \end{aligned} \tag{47}$$

Then, (w^*, b^*) is a degenerate equilibrium of (3) if $\lambda_1 = \lambda_2 = 0$. By the transformation of $u = w - w^*, v = b - b^*$, and still denoted u, v by w, b, (3) becomes

$$\begin{cases} \dfrac{dw}{dt} = \lambda_1 + a_1 w + a_2 b - \lambda w b, \\ \dfrac{db}{dt} = a_3 + b^* w + a_4 b + wb + a_5 b^2 + W_1(w, b), \end{cases}$$

where $W_1(w, b)$ are smooth functions in $w, b, \lambda_1, \lambda_2$ at least of order three, and

$$\begin{aligned} &a_1 = -(\lambda b^* + 1), \qquad a_2 = -\frac{\lambda R_1}{\lambda b^* + 1}, \\ &a_3 = -\frac{b^* \lambda_2}{b^* + 1}, \qquad a_4 = \frac{m_1 b^* - \lambda_2}{(b^* + 1)^2}, \qquad a_5 = \frac{m_1 + \lambda_2}{(b^* + 1)^3}. \end{aligned} \tag{48}$$

Let $u = w, v = \lambda_1 + a_1 w + a_2 b - \lambda w b$ and rewriting u, v as w, b, respectively, we have

$$\begin{cases} \dfrac{dw}{dt} = b, \\ \dfrac{db}{dt} = b_0 + b_1 w + b_2 b + b_3 w^2 + b_4 wb + b_5 b^2 + W_2(w, b), \end{cases}$$

where $W_2(w,b)$ are smooth functions in $w, b, \lambda_1, \lambda_2$ at least of order three, and

$$\begin{aligned}
b_0 &= \frac{a_2^2 a_3 + a_5\lambda_1^2 - a_2 a_4 \lambda_1}{a_2},\\
b_1 &= \frac{b^* a_2^3 - \lambda_1 a_2^2 + a_5\lambda\lambda_1^2 - a_1 a_2^2 a_4 + 2a_1 a_2 a_5\lambda_1 - a_2^2 a_3\lambda}{a_2^2},\\
b_2 &= \frac{\lambda\lambda_1 + a_1 a_2 + a_2 a_4 - 2a_5\lambda_1}{a_2},\\
b_3 &= \frac{a_1^2 a_2^2 a_5 + a_5\lambda^2\lambda_1^2 + 2a_1 a_2 a_5\lambda\lambda_1 - a_1 a_2^3 - \lambda b^* a_2^3}{a_2^3},\\
b_4 &= \frac{\lambda a_1 a_2 + \lambda^2\lambda_1 + a_2^2 - 2a_5\lambda\lambda_1 - 2a_1 a_2 a_5}{a_2^2},\\
b_5 &= \frac{a_5 - \lambda}{a_2}.
\end{aligned} \tag{49}$$

Note that

$$\lim_{(\lambda_1,\lambda_2)\to(0,0)} b_4 = \frac{-\lambda\mu_0^2 + (1-\lambda)(1+2\lambda)\mu_0 + (1-\lambda)^3}{\mu_0(\mu_0\lambda + (1-\lambda)^2)} \neq 0,$$

if $\mu_0 \neq \mu_0^*$.

Setting $u = w + \dfrac{b_2}{b_4}$ and renaming u as w, we have

$$\begin{cases} \dfrac{dw}{dt} = b,\\ \dfrac{db}{dt} = b_0 - \dfrac{b_1 b_2}{b_4} + b_1 w + b_3 w^2 + b_4 w b + b_5 b^2 + W_3(w,b), \end{cases}$$

where $W_3(w,b)$ are smooth functions in $w, b, \lambda_1, \lambda_2$ at least of order three.

Introducing a new time τ by $dt = (1 - b_5 w)d\tau$ and rewriting τ as t, we have

$$\begin{cases} \dfrac{dw}{dt} = b(1 - b_5 w),\\ \dfrac{db}{dt} = (1 - b_5 w)(b_0 - \dfrac{b_1 b_2}{b_4} + b_1 w + b_3 w^2 + b_4 w b + b_5 b^2 + W_3(w,b)). \end{cases}$$

Now, setting $u = w, v = b(1 - b_5 w)$ and renaming u, v as w, b, we obtain

$$\begin{cases} \dfrac{dw}{dt} = b,\\ \dfrac{db}{dt} = c_0 + c_1 w + c_2 w^2 + b_4 w b + W_4(w,b), \end{cases}$$

where $W_4(w,b)$ are smooth functions in $w, b, \lambda_1, \lambda_2$ at least of order three, and

$$\begin{aligned}
c_0 &= b_0 - \frac{b_1 b_2}{b_4}, \qquad & c_1 &= b_1 - 2b_5(b_0 - \frac{b_1 b_2}{b_4})\\
c_2 &= b_3 + b_5^2(b_0 - \frac{b_1 b_2}{b_4}) - 2b_1 b_5.
\end{aligned} \tag{50}$$

Note that

$$\lim_{(\lambda_1,\lambda_2)\to(0,0)} b_0 = 0, \qquad \lim_{(\lambda_1,\lambda_2)\to(0,0)} b_1 = 0,$$

$$\lim_{(\lambda_1,\lambda_2)\to(0,0)} c_2 = \lim_{(\lambda_1,\lambda_2)\to(0,0)} b_3 = \frac{(1-\lambda)b^*}{b^*+1} > 0.$$

Set $u = \dfrac{b_4^2 w}{c_2}, v = \dfrac{b_4^2 b}{c_2^2}, \tau = \dfrac{c_2 t}{b_4}$, and denote u, v, τ as w, b, t, respectively. We have

$$\begin{cases} \dfrac{dw}{dt} = b, \\ \dfrac{db}{dt} = \eta_1 + \eta_2 w + w^2 + wb + W_5(w, b), \end{cases}$$

where $W_5(w, b)$ are smooth functions in $w, b, \lambda_1, \lambda_2$ at least of order three, and

$$\eta_1 = \frac{c_0 b_4^4}{c_2^3}, \qquad \eta_2 = \frac{c_1 b_4^2}{c_2^2}.$$

By the results of Section 8.4.2 in [16], we have the following approximating bifurcation curves in a small neighborhood of the origin.

Theorem A.1. *Assume a_k, b_k, c_k are defined as (48), (49) and (50), respectively. Suppose that (C_1) and (C_2) hold and $\mu_0 \neq \mu_0^*$. Then*

1. *there is a saddle-node bifurcation curve $SN : \{(\lambda_1, \lambda_2) : 4c_0c_2 = c_1^2 + o(\|\mu\|^2)\}$;*
2. *there is a Hopf bifurcation curve $H : \{(\lambda_1, \lambda_2) : c_0 = 0 + o(\|\mu\|^2)\}$;*
3. *there is a homoclinic bifurcation curve $HL : \{(\lambda_1, \lambda_2) : 25c_0c_2 + 6c_1^2 = 0 + o(\|\mu\|^2)\}$.*

Here, $\mu = (\lambda_1, \lambda_2)$.

Acknowledgments. The authors wish to express their grateful thanks to the anonymous referees for their careful reading and some valuable comments and suggestions which greatly improved this work. X.-L. Wang and G.-H. Zhang would like to thank all the members of College of William and Mary for their support and hospitality during their visit.

REFERENCES

[1] J. C. Alexander and J. A. Yorke, Global bifurcations of periodic orbits, *Amer. J. Math.*, **100** (1978), 263–292.

[2] J. Arino, C. C. McCluskey and P. van den Driessche, Global results for an epidemic model with vaccination that exhibits backward bifurcation, *SIAM J. Appl. Math.*, **64** (2003), 260–276.

[3] F. Brauer and C. Castillo-Chávez, *Mathematical Models in Population Biology and Epidemiology*, volume 40 of Texts in Applied Mathematics, Springer, New York, 2012.

[4] S. R. Carpenter and W. A. Brock, Rising variance: A leading indicator of ecological transition, *Ecol. Lett.*, **9** (2006), 311–318.

[5] S.-N. Chow and J. Mallet-Paret, The Fuller index and global Hopf bifurcation, *J. Differential Equations*, **29** (1978), 66–85.

[6] E. Gilad, M. Shachak and E. Meron, Dynamics and spatial organization of plant communities in water-limited systems, *Theor. popul. biol.*, **72** (2007), 214–230.

[7] E. Gilad, J. von Hardenberg, A. Provenzale, M. Shachak and E. Meron, Ecosystem engineers: From pattern formation to habitat creation, *Phys. Rev. Lett.*, **93** (2004), 098105.

[8] J. Guckenheimer and P. Holmes, *Nonlinear Oscillations, Dynamical Systems, and Bifurcations of Vector Fields*, volume 42 of Applied Mathematical Sciences, Springer-Verlag, New York, 1983.

[9] K. P. Hadeler and P. van den Driessche, Backward bifurcation in epidemic control, *Math. Biosci.*, **146** (1997), 15–35.

[10] S.-B. Hsu and T.-W. Huang, Global stability for a class of predator-prey systems, *SIAM J. Appl. Math.*, **55** (1995), 763–783.

[11] S.-B. Hsu and T.-W. Huang, Uniqueness of limit cycles for a predator-prey system of Holling and Leslie type, *Canad. Appl. Math. Quart.*, **6** (1998), 91–117.

[12] C. G. Jones, J. H. Lawton and M. Shachak, Organisms as ecosystem engineers, *Ecosystem Management*, 1996, 130–147.

[13] C. G. Jones, J. H. Lawton and M. Shachak, Positive and negative effects of organisms as physical ecosystem engineers, *Ecology*, **78** (1997), 1946–1957.

[14] C. A. Klausmeier, Regular and irregular patterns in semiarid vegetation, *Science*, **284** (1999), 1826–1828.

[15] A. J. Koch and H. Meinhardt, Biological pattern formation: From basic mechanisms to complex structures, *Rev. Mod. Phys.*, **66** (1994), 1481–1507.

[16] Y. A. Kuznetsov, *Elements of Applied Bifurcation Theory*, volume 112 of Applied Mathematical Sciences, Springer-Verlag, New York, 1998.

[17] R. Lefever and O. Lejeune, On the origin of tiger bush, *Bull. Math. Biol.*, **59** (1997), 263–294.

[18] R.-S. Liu, Z.-L. Feng, H.-P. Zhu and D. L. DeAngelis, Bifurcation analysis of a plant-herbivore model with toxin-determined functional response, *J. Differential Equations*, **245** (2008), 442–467.

[19] M.-X. Liu, E. Liz and G. Röst, Endemic bubbles generated by delayed behavioral response: Global stability and bifurcation switches in an SIS model, *SIAM J. Appl. Math.*, **75** (2015), 75–91.

[20] A. Manor and N. M. Shnerb, Dynamical failure of Turing patterns, *Europhys. Lett.*, **74** (2006), 837–843.

[21] R. M. May, Thresholds and breakpoints in ecosystems with a multiplicity of stable states, *Nature*, **269** (1977), 471–477.

[22] H. Meinhardt, Pattern formation in biology: A comparison of models and experiments, *Rep. Prog. Phys.*, **55** (1992),797–849.

[23] E. Meron, E. Gilad and J. von Hardenberg, et al, Vegetation patterns along a rainfall gradient, *Chaos, Solitons Fract.*, **19** (2004), 367–376.

[24] L. Perko, *Differential Equations and Dynamical Systems*, volume 7 of Texts in Applied Mathematics, Springer-Verlag, New York, 2001.

[25] M. Rietkerk, S. C. Dekker, P. C. De Ruiter and J. van de Koppel, Self-organized patchiness and catastrophic shifts in ecosystems, *Science*, **305** (2004), 1926–1929.

[26] M. Scheffer, J. Bascompte and W. A. Brock, et al, Early-warning signals for critical transitions, *Nature*, **461** (2009), 53–59.

[27] M. Scheffer, S. Carpenter and J. A. Foley, et al, Catastrophic shifts in ecosystems, *Nature*, **413** (2001), 591–596.

[28] N. M. Shnerb, P. Sarah, H. Lavee and S. Solomon, Reactive Glass and Vegetation Patterns, *Phys. Rev. Lett.*, **90** (2003), 038101.

[29] H.-Y. Shu, L. Wang and J.-H. Wu, Global dynamics of Nicholson's blowflies equation revisited: Onset and termination of nonlinear oscillations, *J. Differential Equations*, **255** (2013), 2565–2586.

[30] A. M. Turing, The chemical basis of morphogenesis, *Philos. Trans. R. Soc. Lond. B Biol. Sci.*, **237** (1952), 37–72.

[31] J. von Hardenberg, E. Meron, M. Shachak and Y. Zarmi, Diversity of vegetation patterns and desertification, *Phys. Rev. Lett.*, **87** (2001), 198101.

[32] J.-L. Wang, S.-Q. Liu, B.-W. Zheng, and Y. Takeuchi, Qualitative and bifurcation analysis using an SIR model with a saturated treatment function, *Math. Comput. Modelling*, **55** (2012), 710–722.

[33] J.-F. Wang, J.-P. Shi and J.-J. Wei, Predator-prey system with strong Allee effect in prey, *J. Math. Biol.*, **62** (2011), 291–331.

[34] W.-D. Wang, Backward bifurcation of an epidemic model with treatment, *Math. Biosci.*, **201** (2006), 58–71.

[35] W.-D. Wang and S.-G. Ruan, Bifurcation in an epidemic model with constant removal rate of the infectives, *J. Math. Anal. Appl.*, **291** (2004), 775–793.

[36] X.-L. Wang, W.-D. Wang and G.-H. Zhang, Global analysis of predator-prey system with hawk and dove tactics, *Stud. Appl. Math.*, **124** (2010), 151–178.

[37] A. S. Watt, Pattern and process in the plant community, *J. Ecol.*, **35** (1947), 1–22.

[38] X. Zhang and X.-N. Liu, Backward bifurcation of an epidemic model with saturated treatment function, *J. Math. Anal. Appl.*, **348** (2008), 433–443.

[39] L.-H. Zhou and M. Fan, Dynamics of an SIR epidemic model with limited medical resources revisited, *Nonlinear Anal. Real World Appl.*, **13** (2012), 312–324.

Received April 2016; revised April 2017.

E-mail address: wxl711@swu.edu.cn
E-mail address: shij@math.wm.edu
E-mail address: zgh711@swu.edu.cn